



UNIVERSITÀ  
DEGLI STUDI  
FIRENZE

# FLORE

## Repository istituzionale dell'Università degli Studi di Firenze

### **Finite element modelling for seismic assessment of historic masonry buildings**

Questa è la Versione finale referata (Post print/Accepted manuscript) della seguente pubblicazione:

*Original Citation:*

Finite element modelling for seismic assessment of historic masonry buildings / Betti, Michele; Galano, Luciano; Vignoli, Andrea. - STAMPA. - (2016), pp. 377-416. [10.1007/978-3-319-21753-6\_14]

*Availability:*

This version is available at: 2158/1016975 since: 2017-05-23T16:08:12Z

*Publisher:*

Springer International Publishing

*Published version:*

DOI: 10.1007/978-3-319-21753-6\_14

*Terms of use:*

Open Access

La pubblicazione è resa disponibile sotto le norme e i termini della licenza di deposito, secondo quanto stabilito dalla Policy per l'accesso aperto dell'Università degli Studi di Firenze (<https://www.sba.unifi.it/upload/policy-oa-2016-1.pdf>)

*Publisher copyright claim:*

(Article begins on next page)

# Finite Element Modelling for Seismic Assessment of Historic Masonry Buildings

Michele Betti, Luciano Galano and Andrea Vignoli

## 1 Introduction

A large portion of the European cultural heritage is made of masonry buildings that have a growing economic and social value in many countries. Therefore, their preservation is considered an important issue in modern societies both for their historical interest and for the economic contribution in contexts where tourism has become a major industry (Bowitz and Ibenholt 2009). During past and recent earthquakes (Lucibello et al. 2013; Ceci et al. 2013; Brandonisio et al. 2013) these historic buildings have demonstrated to be particularly prone to damage, showing partial or total collapse. In many cases, this was due to restorations non-respectful of the original structural layout (Ramos and Lourenço 2004; Borri et al. 2000). Generally, masonry buildings are capable of carrying out vertical loads in a safe and stable way, while they are rather sensitive to horizontal loads such as the seismic ones. The high seismic vulnerability of these buildings is due both to their particular structural configuration and to the mechanical properties of the masonries. Open spaces, slender walls, lack of effective connections among the structural elements and the highly nonlinear behaviour with very small tensile strength are some examples of structural and material lacks.

In principle, prediction of the structural behaviour of a monumental building is similar to that of other constructed facilities. However, the analysis of an historic building is an even more challenging task (Del Piero 1984; Carpinteri et al. 2005;

---

M. Betti (✉) · L. Galano · A. Vignoli  
Department of Civil and Environmental Engineering (DICEA),  
University of Florence, Via di Santa Marta, 3, 50139 Florence, Italy  
e-mail: mbetti@dicea.unifi.it

L. Galano  
e-mail: luciano@dicea.unifi.it

A. Vignoli  
e-mail: avignoli@dicea.unifi.it

Bartoli and Betti 2013) and, in some cases, train to extrapolate analytical procedures specifically developed for modern buildings is inadequate. A correct structural evaluation should be based on a deep knowledge of: (i) the history of the building and its evolution, (ii) the geometry, (iii) the structural details, (iv) the cracking pattern and the material damage map, (v) the masonry constructive technique, (vi) the material properties, and (vii) the global behaviour (Siviero et al. 1997; Leftheris et al. 2006). This knowledge can be reached through both in situ and laboratory experimental investigations (Corradi et al. 2002a, b; Binda et al. 2000) joined with structural analyses with appropriate models (Lourenço et al. 2007). Nevertheless, the restrictions set on inspections and on performing reliable quantitative strength evaluations results in limited information on the constructive system and properties of the materials.

These issues have been recently addressed by the Italian Guidelines for seismic vulnerability assessment of cultural heritage (DPCM 2011) that introduce the concept of knowledge level (KL) for monumental buildings specifying the confidence factor (CF) obtained through in situ tests and investigations. These Guidelines propose a methodology of analysis based on three different levels of evaluation, according to an increasing knowledge of the structure. The first level of analysis (Level 1, LV1) allows to evaluate the collapse acceleration of the structure by means of simplified models based on a limited number of geometrical and mechanical parameters (and qualitative tools such as visual inspections). The second level (Level 2, LV2) is based on a kinematic approach performed to analyse the local collapse mechanisms that can develop on several macro-elements. The identification of proper macro-elements is based on the knowledge of structural details of the building (cracking pattern, connections between the architectonic elements, etc.). The last level of evaluation (Level 3, LV3) requires a global analysis of the whole building under seismic loading by suitable numerical models.

Each level of evaluation should be appropriate with the achieved knowledge level. Usually, the LV1 level is a simplified territorial or urban scale seismic assessment performed on the whole building. The aim is to provide general guidelines to establish priority of interventions for the protection of historic monuments. The LV2 level provides the horizontal load multiplier that activates the local collapse of each macro-element considered. This level has to be considered when the structure needs of local interventions. The LV3 level is required in the case of global seismic assessment or interventions that modify the whole structural behaviour. This evaluation is usually performed by means of a finite element model of the structure in which the seismic action is considered performing static or dynamic nonlinear analyses. Compared to the previous two levels the LV3 is the most accurate, but it requires large amount of input data and great computational effort.

The above issues enlighten the attention that must be paid in modelling strategies of historic masonry constructions. Each monumental building is, by definition, a unique building characterised by its own history, often resulting in a composite mixture of added or replaced, strongly interacting, structural elements. Hence, engineers involved in the study of cultural heritage are called to have a specific care

in the understanding of the historical process since modifications occurred through the building history produced several uncertainties in the model definition.

In this respect, the scientific literature presents a significant number of exemplary case studies that cover a wide range of applications around the European Community. Lourenço (2005) analyses the Church of Saint Christ in Outeiro (Bragança, North of Portugal). The papers show that sophisticated tools of structural analysis offer significant information for both understanding the existing damage and designing the strengthening of ancient structures. Romera et al. (2008a, b) analyse the Basilica of Pilar in Zaragoza, one of the most famous Spanish temples. The authors identify the actual structural state of the Church, its safety level and the relationship between structural behaviour and actual damage. A global numerical model of the Church was built and the masonry was simulated as a nonlinear material with brittle behaviour in tension and plastic properties in compression. The authors take in consideration the construction steps, including the reinforcement works added to the structure. The paper shows that suitable numerical models can offer effective information in both reproducing structural pathologies and check out the efficiency of historic restoration. Another example is presented by Lourenço et al. (2007). The authors investigate the structural safety of the Monastery of Jeronimos in Lisbon (Portugal). The paper advocates that the computational models can be used as a numerical laboratory, where the sensitivity of the results to the input material parameters and boundary conditions can be efficiently analysed, offering effective information in the design of in situ testing and structural monitoring. Betti and Vignoli (2008) analyse a Romanesque church, the Abbey of Farneta near Cortona (Italy). The authors build a 3D numerical model of the monument and develop linear and nonlinear analyses to assess the seismic vulnerability and the efficiency of traditional strengthening techniques. Taliercio and Binda (2008) analyse the Basilica of San Vitale in Ravenna (Italy), a Byzantine building which suffers diffused cracking and excessive deformations. The authors take into account the results of in situ topographical and mechanical investigations and build a global finite element model of the Basilica conceived as a first step toward the understanding of the structural behaviour. Ivorra et al. (2009) assess the seismic behaviour of the San Nicolas Bell Tower in Valencia (Spain). The finite element model of the Tower was first calibrated by means of in situ dynamic tests and subsequently used to evaluate the seismic response with respect to the seismic Spanish standards. The numerical simulations showed a satisfactory performance of the Tower. Del Coz Diaz et al. (2007) analyse the Palatine Chapel of San Salvador de Valdediós near Oviedo (Spain) and combine the finite element method with a frictional contact problem. The analyses were based on the application of the finite element technique to each stone block, and the blocks were assembled side by side using contact elements in order to reproduce the mechanical behaviour of the mortar. The authors show that sophisticated analysis tools provide a clear understanding of the structural behaviour. Betti et al. (2010) analyse the cracking pattern of a historic Italian palace and show a careful use of the finite element technique when dealing with practical engineering problems. The authors provide an interpretation of the manifested damage in the palace, and use the numerical results to

design an extensive in situ investigation on the building. Ivorra et al. (2010) report a study carried out on the Bell Tower of the Church of Santas Justa and Rufina in Orihuela in Alicante (Spain). The model was first calibrated based on the dynamic characteristics in free vibration and then used to predict the evolution of the dynamic behaviour of the Bell Tower, considering the subsidence caused by variations in water table level.

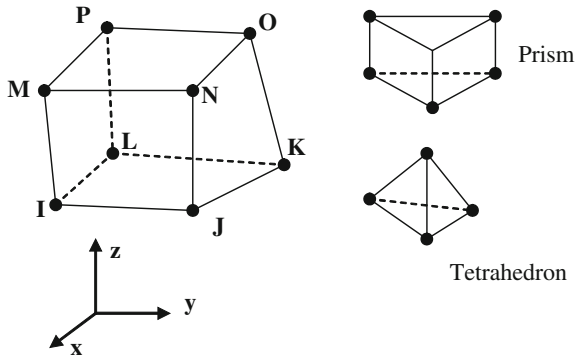
Within this field of research the chapter focused the attention to some aspects of numerical modelling, to offer a contribution to the analysis of historic masonry buildings under seismic actions. The chapter is hence organized as follows. In the first part a numerical model used to replicate the nonlinear behaviour of the masonry is described. The model is quite general and is herein discussed with specific reference to the commercial finite element code ANSYS (1998). The identification of the required parameters is discussed using the results of experimental tests performed in old masonry buildings. In a second part the above approach is employed to build a finite element model of two relevant case studies and to analyse their seismic behaviour. The two examples illustrate the use of numerical analyses to face practical engineering problems in the field of seismic assessment of historic constructions.

## **2 The Numerical Model of Masonry**

### ***2.1 Modelling Approach***

Masonry is an anisotropic non-homogeneous and nonlinear material composed by units (bricks and/or stones) and mortar joints. So, the modelling depends both on dimensions and arrangement of the units and on the size of the joints. According to the approaches proposed in literature, the numerical models can be performed with two different levels of detail (Zucchini and Lourenço 2002; Theodossopoulos and Sinha 2013). In the so-called micro-modelling approach, units and mortar joints are represented by continuous elements and are modelled separately. Discontinuous elements represent the interfaces between units and mortar. Since all material characteristics of the components are considered separately, this modelling strategy correctly reflects the actual behaviour of the masonry when experimental data are available for each component. A simplified version of the micro-modelling approach makes use of interface elements to account for both mortar joints and contacts between units and mortar. The units are still modelled as continuous elements (Gambarotta and Lagomarsino 1997; Da Porto et al. 2010). The micro-modelling approach (detailed or simplified) is usually employed to analyse specific problems of little-size since, it is hardly computational demanding in the application to large structures. For large-size models the so-called macro-modelling approach is the most commonly employed technique. Bricks, mortar joints and interfaces are globally represented by single continuous elements. The mechanical properties of the homogenous elements depend on those of the basic components.

**Fig. 1** Geometry, node locations and coordinate system for the *Solid65* element



Proper homogenisation techniques (Zucchini and Lourenço 2007) and experimental setup were accordingly proposed to determine these average parameters. This approach is appropriate to analyse large or complex structures, because the calculation is less demanding. Another field of application of the macro-modelling strategy is represented by the structural masonries with *opus incertum* texture.

Taking into account that the chapter aims at discussing the finite element (FE) modelling technique for the seismic assessment of historic masonry structures, the macro-modelling approach is considered. Specifically, 8-nodes isoparametric finite elements having three degrees of freedom at each node (*Solid65*) were employed to model the masonry assemblages (Fig. 1).

## 2.2 The Elastoplastic Model

In the follows it is considered a material with isotropic behaviour, according to the chaotic texture of the masonry in many existing historic buildings. The elastic behaviour of the equivalent continuum is ruled by the following classical equations:

$$\{\dot{\sigma}\} = \mathbf{E}\{\dot{\varepsilon}\}^{el} = \mathbf{E}\left(\{\dot{\varepsilon}\} - \{\dot{\varepsilon}\}^{pl}\right) \tag{1}$$

$$E_{ijkl} = \left(K - \frac{2}{3}G\right)\delta_{ij}\delta_{kl} + G(\delta_{ik}\delta_{jl} + \delta_{il}\delta_{jk}) \tag{2}$$

$$G = \frac{E}{2(1 + \nu)}; \quad K = \frac{E}{3(1 - 2\nu)} \tag{3}$$

where  $E$  and  $G$  denote the longitudinal and the tangential modules of elasticity,  $K$  denotes the bulk modulus and  $\nu$  is the Poisson's ratio.  $\{\sigma\}$  and  $\{\varepsilon\}$  denote the stress and the total strain tensor, respectively. Dots indicate the incremental formulation of the law. To characterize the elastic stress-strain rule of a homogeneous and isotropic material only two constants are required. The plastic law, that

characterizes the material behaviour over the elastic range, requires the definition of the following three conditions:

- a yield function that bounds the elastic domain (which identifies the condition at which the plastic flow begins);
- a rule of plastic flow, which correlates the increase of plastic deformation  $\{\hat{\varepsilon}\}^{pl}$  to the current state of stress;
- a hardening rule that modifies the yield function during the plastic flow.

Taking into account the available material laws in the ANSYS code, these requirements are accomplished assuming the Drucker-Prager (DP) plasticity material model (ANSYS 1998; Drucker and Prager 1952). This is typically employed for pressure-dependent inelastic materials such as soils, rocks and concretes, and it is a modification of the Von Mises yield criterion that accounts for the hydrostatic stress component (the confinement pressure). The yield surface of the DP plasticity criterion depends on the first and the second invariant of the stress tensor and remains fixed in the stress space. Usually, the invariants considered to express the yield surface are the mean hydrostatic stress  $\sigma_m$  and the effective shear stress  $\bar{\sigma}$ :

$$\bar{\sigma}^2 = \frac{1}{2} s_{ij} s_{ij}; \quad \sigma_m = \frac{\sigma_{ii}}{3} \quad (4)$$

where  $s_{ij}$  are the deviatoric components of the stress tensor  $\sigma_{ij}$ . The DP yield condition is defined as follows:

$$F = 3\alpha \sigma_m + \bar{\sigma} - k = 0 \quad (5)$$

The constants  $\alpha$  and  $k$  are two parameters related to the friction angle  $\varphi$  and to the cohesion  $c$  of the material, according to the following equations:

$$\alpha = \frac{2 \sin \varphi}{\sqrt{3}(3 - \sin \varphi)}; \quad k = \frac{6c \cos \varphi}{\sqrt{3}(3 - \sin \varphi)} \quad (6)$$

The two parameters  $\alpha$  and  $k$  allow to evaluate the yield stresses in uniaxial tension and compression,  $f_{iDP}$  and  $f_{cDP}$  respectively, by:

$$f_{iDP} = \frac{k}{\frac{1}{\sqrt{3}} + \alpha}; \quad f_{cDP} = \frac{k}{\frac{1}{\sqrt{3}} - \alpha} \quad (7)$$

In case of elastic-perfectly plastic behaviour, the friction angle  $\varphi$  and the cohesion  $c$  are constant and do not depend on the plastic deformation. The normal to the yield surface is calculated as follows:

$$\mathbf{Q} = \frac{\partial F}{\partial \sigma} = \alpha \delta_{ij} + \frac{1}{2\bar{\sigma}} s_{ij} \quad (8)$$

The flow rule, that determines the direction of the plastic straining, is hence given as:

$$\{\dot{\epsilon}\}^{pl} = \langle \lambda \rangle \mathbf{P}; \quad \mathbf{P} = \beta \delta_{ij} + \frac{1}{2\sigma} s_{ij}; \quad \langle \lambda \rangle = \frac{1}{2} (\lambda + |\lambda|) \quad (9)$$

being  $\mathbf{P}$  the plastic potential. If it is assumed  $\alpha = \beta$  (then  $\mathbf{P} = \mathbf{Q}$ ) the flow rule is called associated and the plastic straining occurs in direction normal to the yield surface. The experimental results available for soils and rocks show that the volumetric dilatation predicted by the associated DP flow rule is often larger than that obtained by the experiments. Therefore, a non-associated flow rule should be used through a proper definition of the plastic potential. In the present case a third parameter for the DP plasticity behaviour is introduced, called dilatancy angle  $\delta$ . This parameter rules the flow degree of associativity. If  $\delta = \varphi$  the flow is associated, whereas if  $\delta = 0$  no plastic volumetric strains will be produced. In conclusion, the definition of the DP model requires three parameters: the friction angle  $\varphi$  that describes the slope of the yield surface (if  $\varphi = 0$  there is no dependence on the hydrostatic pressure), the cohesion  $c$  (the yield strength at zero hydrostatic pressure) and the dilatancy angle  $\delta$ .

The DP yield surface can be considered as a smooth version of the Mohr-Coulomb yield surface, and usually the parameters  $c$  and  $\varphi$  are introduced in such a way that the circular cone of DP corresponds to the outer vertex of the hexagonal Mohr-Coulomb yield surface. The resulting surface is a right-circular cone with apex at  $\rho = k/\sqrt{3}\alpha$  (Fig. 2).

Depending on the parameter  $\alpha$  and on the ratio  $f_{IDP}/f_{cDP}$ , the yield function, for the plane stress, has three conical forms: elliptic, parabolic and hyperbolic. These forms can be effectively analysed in the two-dimensional space ( $\sigma_{III} = 0$ ), considering the cross-section of the DP cone in the plane ( $\sigma_I, \sigma_{II}$ ). Taking into account that for masonry the ratio between the uniaxial compressive and tensile strengths is usually greater than 3, it is obtained  $\alpha^2 > 1/12$  and the conical form of the intersection is parabolic (Fig. 3).

**Fig. 2** Drucker-Prager yield surface in the Haigh-Westergaard stress space

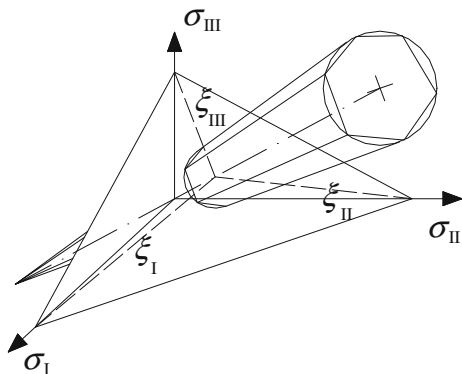
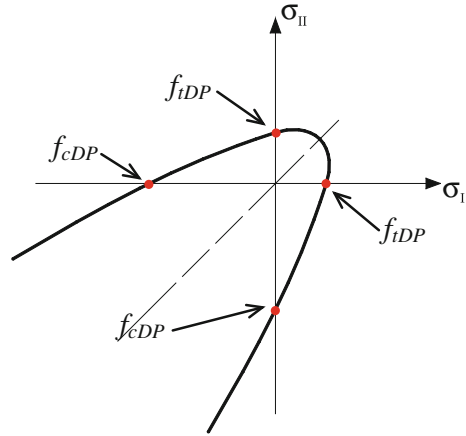




**Fig. 3** Cross-section of the Drucker-Prager cone with the plane  $(\sigma_I, \sigma_{II})$  when  $\alpha^2 > 1/12$



### 2.3 The Smeared Crack Model

A smeared crack model is introduced through the definition of a crushing and cracking rule. The model makes use of the failure surface employed in ANSYS for concrete and proposed by Willam and Warnke (WW) (William and Warnke 1975; Salari et al. 2004; Hansen et al. 2001). According to this criterion the element is capable of cracking in tension and crushing in compression. The failure surface shows an elliptic trace on the deviatoric sections in each sextant, and a parabolic trace in the meridian sections (Fig. 4).

The WW surface is defined by five parameters: the uniaxial compressive strength  $f_{cWW}$ , the uniaxial tensile strength  $f_{tWW}$ , the biaxial compressive strength  $f_{cb}$  and, two additional parameters  $\rho_1$  and  $\rho_2$ . The last two parameters define the curvature of the parabolic traces in the meridian sections for high values of the hydrostatic compression, for anomalies  $\zeta = 0^\circ$  and  $\zeta = 60^\circ$ . The failure surface is characterized by

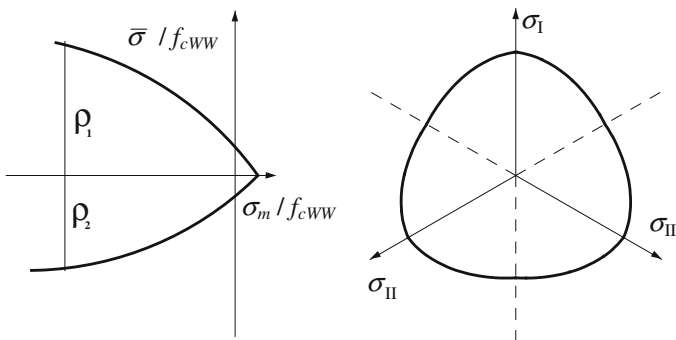


**Fig. 4** Hydrostatic section of the yield surface (left) and section across a deviatoric plane (right)

proper expressions into four domains: CCC, CCT, CTT and TTT (C = compression, T = tension). In the CCC zone, f.i., this surface can be expressed as follows:

$$F' = \frac{1}{r(\sigma_m, \zeta)} \sqrt{\frac{3}{5}} \frac{\bar{\sigma}}{f_{cWW}} - 1 = 0 \quad (10)$$

where  $r$  and  $\zeta$  are the polar coordinates (radius vector and anomaly) of the representative point of the stress state in the deviatoric plane. The criterion accounts for both cracking and crushing failure modes through a smeared model and the crisis surface is completed by cut-off conditions. At each Gauss point cracking is permitted in three orthogonal directions and is modelled by modifying the material properties of the element introducing a plane of weakness normal to the crack face. It is worth nothing that the model is a fixed crack model.

Despite the need for five constants, in most practical cases (thereby when the hydrostatic stress is limited by  $\sqrt{3}f_{cWW}$ ) the definition of the failure surface can be specified by means of only two constants,  $f_{iWW}$  and  $f_{cWW}$ , since the three other constants can be assumed as follows:

$$f_{cb} = 1.2f_{cWW}, \quad \rho_1 = 1.45f_{cWW}, \quad \rho_2 = 1.725f_{cWW} \quad (11)$$

The model allows for the introduction of two additional coefficients, denoted as  $\beta_t$  and  $\beta_c$ , that account for a shear strength reduction of the stress producing sliding across the crack face for open ( $\beta_t$ ) or re-closed cracks ( $\beta_c$ ) (ANSYS 1998).

The WW failure criterion can be joined with the DP plasticity criterion and as a result, the material behaves as an isotropic medium with plastic deformation, cracking and crushing capabilities. The parameters required are the following:

- elastic parameters:  $E$  and  $\nu$ ;
- plastic parameters (DP):  $c$ ,  $\varphi$  and  $\delta$ ;
- cracking and crushing parameters (WW):  $f_{cWW}$ ,  $f_{iWW}$ ,  $\beta_t$  and  $\beta_c$ .

The combination of the two models requires a careful definition of the above parameters. According to the experimental evidence such choice must comply with the following criteria:

- the tensile strength  $f_{iWW}$  must be smaller than the tensile strength derived from the plasticity model  $f_{iDP}$ ;
- the compressive strength  $f_{cWW}$  must be greater than the compressive strength derived from the plasticity model  $f_{cDP}$ , to ensure the correct plastic behaviour of the masonry in the mixed tensile-compression zone.

The proper combination of these parameters allows for an elastic-brittle behaviour in case of biaxial tensile stresses or biaxial tensile-compressive stresses with low compression level. On the contrary, the material is elastoplastic in case of biaxial compressive stresses or biaxial tensile-compressive stresses with high compression level.

Both the DP and the WW criteria have been extensively employed in the scientific literature to model the inelastic behaviour of masonry assemblages. Discussing the homogenisation approach for masonry Zucchini and Lourenço (2007) adopt the DP model for the simulation of the plastic deformation in masonry cells. They show that it is possible to account for the degradation of the masonry mechanical properties in compression. The DP criterion was adopted by Cerioni et al. (1995) to discuss the seismic behaviour of the Parma Cathedral Bell-Tower. Adam et al. (2009) used the WW criterion to model cracking and crushing phenomena, and the comparison between numerical and experimental results showed a good agreement. Chiostrini et al. (1998) combine the DP and the WW criteria to model the results of several diagonal tests on masonry panels, obtaining good agreement with the experimental results. Betti and Vignoli (2008) combine the two criteria to discuss the seismic vulnerability of a masonry church.

The assignment of the mechanical parameters required by the DP and the WW criteria requires a careful calibration (Chiostrini et al. 1998). The following section discusses the identification of these parameters through the results of experimental investigations.

### 3 Tuning of the Numerical Model

#### 3.1 *Experimental Tests*

The constitutive parameters of the model should be evaluated on the basis of the in situ mechanical properties of the masonry walls. This requires to perform a set of experimental investigations. The paragraph discusses some of the tests that can be performed on masonry panels to evaluate the required parameters, and shows a calibration of the model based on these tests. It is worth noting that the difficulties in removing specimens in buildings of historic value suggest the calibration of the parameters using experimental results available from similar masonry textures. Herein, for illustrative purposes, the results of past experimental researches (Chiostrini and Vignoli 1992, 1994; Chiostrini et al. 2000, 2003) aimed to assess both strength and deformability of masonry walls of historic masonry buildings in Tuscany (Central Italy) are discussed.

The experimental researches comprehended laboratory tests on masonry samples and destructive in situ tests on masonry panels. The in situ tests were: direct shear tests (S), shear-compression tests (SC) and diagonal compression tests (DC). The first two types of test reproduce with good approximation the stress state of a masonry pier under seismic loading. The third test is useful for a direct evaluation of the masonry tensile strength. In a first experimental campaign (Chiostrini and Vignoli 1992, 1994) S and SC tests were performed on nine panels selected from different buildings: the S. Orsola Monastery in the historic centre of Florence (four panels: T1, T2, T3 and T4), an old residential building in Florence (three panels: COR1, COR2 and COR3) and two buildings in Pontremoli (Lunigiana, Central

Tuscany), the Istituto Belmesseri and the Town Hall (one panel for each case: BEL and COM). Common characteristics of these buildings were: bearing walls made with stone or mixed stone and brick masonry with chaotic textures and wood floor slabs with insufficient linkage between slabs and walls. Thickness of the panels varied from about 300 to 600 mm.

In a second experimental investigation (Chiostrini et al. 2000, 2003) three shear-compression tests and four diagonal compression tests were performed on seven masonry panels selected in five different rural buildings. Common characteristics of these buildings were: two or three stories height, bearing walls made by stone masonry with typical chaotic textures and wood or steel floor slabs.

Figures 5 and 6 show the experimental setup of the direct shear test (S) and the shear-compression test (SC). After having isolated the masonry panel under

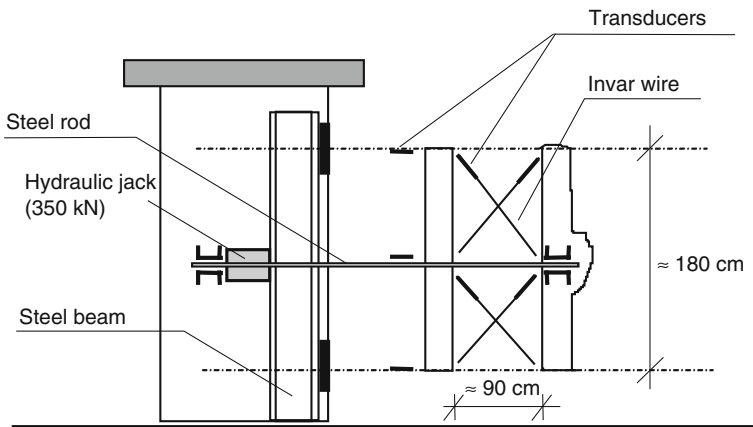


Fig. 5 Experimental setup of the direct shear test (S)

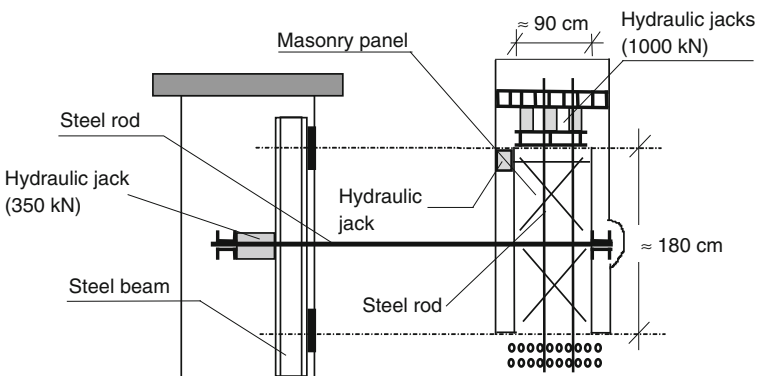


Fig. 6 Experimental setup of the shear-compression test (SC)

**Table 1** In-situ direct shear and shear-compression tests on masonry panels

Panel ID	Location	Building	Panel cross-section (cm <sup>2</sup> )	In-situ test	Masonry texture
T1	Florence	S. Orsola	4503	SC	SO1
T2	Florence	S. Orsola	4536	SC	SO2
T3	Florence	S. Orsola	4648	SC	SO2
T4	Florence	S. Orsola	3669	SC	SO1
COR1	Florence	Residential	2640	S	VC
COR2	Florence	Residential	2760	S	VC
COR3	Florence	Residential	2511	S	VC
BEL	Pontremoli	Ist. Belmesseri	4480	S	Bel
COM	Pontremoli	Town hall	2880	S	Com
A	Pieve Fosciana	Town hall	5765	SC	PF
B	Pieve Fosciana	Town hall	4798	SC	PF
E	Pognana	Residential	5400	SC	Po

*SO1* = mixed stone and brick masonry with chaotic texture; *SO2* = mixed stone and brick masonry with regular texture; *VC* = mixed stone and brick masonry with chaotic texture; *Bel* = stone and brick infilled masonry with chaotic texture; *Com* = stone infilled masonry with chaotic texture; *PF* = two facings stone wall compact and interlocked; *Po* = two facings stone wall with irregular masonry texture infilled with packed mortar

investigation from the rest of the wall through two vertical cuts, the direct shear test is performed applying a horizontal force until the panel collapses. During the test the values of the deformations of the two main diagonals (the one in compression and the one in tension) of the panels are acquired. The deflection of the specimen in the middle section is also monitored. The shear-compression test is similar to the previous, but in this case a vertical pressure is firstly applied through hydraulic actuators (steel plates are positioned over the panel to apply a uniform compressive stress). Table 1 reports a summary of the performed S and SC tests. The table shows: an identification code of the panel (ID), the location, the type of building, the area of the cross-section of the panel, the type of test (S or SC) and a brief description of the masonry texture (thickness of the masonry panels was variable from about 300 to 600 mm).

Results of S and SC tests are summarised in Table 2 where the following data are collected: the vertical pressure acting on the panel  $\sigma_0$ , the characteristic shear strength  $\tau_k$  and the value of the *b* shape factor employed for the calculation of  $\tau_k$ . In addition, the table reports the values of the elastic tangential modulus *G* obtained through the shear-strain curve of the elastic range part of the tests, and the elastic longitudinal modulus *E* obtained in the preliminary tests. It is possible to observe the high variability of the mechanical properties of these masonries.

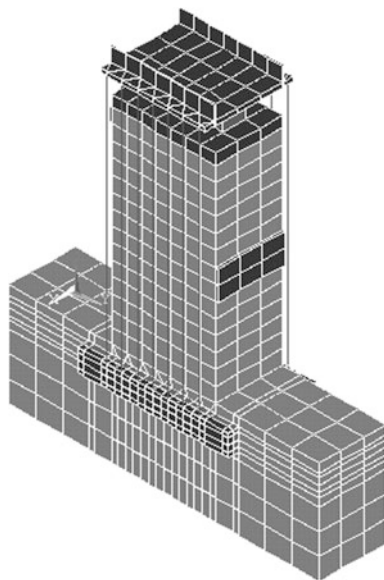
**Table 2** Results of the experimental in-situ tests

Panel ID	$\sigma_0$ (N/mm <sup>2</sup> )	$\tau_k$ (N/mm <sup>2</sup> )	$b$	$E$ (N/mm <sup>2</sup> )	$G$ (N/mm <sup>2</sup> )
T1	0.800	0.114	1.37	/	200
T2	0.800	0.090	1.40	/	116
T3	0.400	0.109	1.29	/	274
T4	0.400	0.170	1.19	/	241
COR1	0.230	0.081	1.23	/	173
COR2	0.430	0.090	1.33	/	325
COR3	0.120	0.197	1.0	/	333
BEL	0.190	0.096	1.14	/	290
COM	0.130	0.203	1.0	/	249
A	0.378	0.234	1.0	1468	179
B	0.433	0.320	1.0	1333	435
E	0.165	0.065	1.21	250	102

### 3.2 Identification of Model Parameters

The direct shear tests on panels COR2, BEL and COM and the shear-compression tests on panels A and B were used to identify the model parameters. The setup of both tests was modelled using the finite element *Solid65* (Fig. 1) and two cases were considered. In the first case only the plasticity model was accounted for, in the second case both the plasticity and the failure model were considered. As an example, Fig. 7 shows the FE model used for the simulation of the SC test on panel

**Fig. 7** FE model of the shear-compression test on panel B in Pieve Fosciana (Lunigiana)



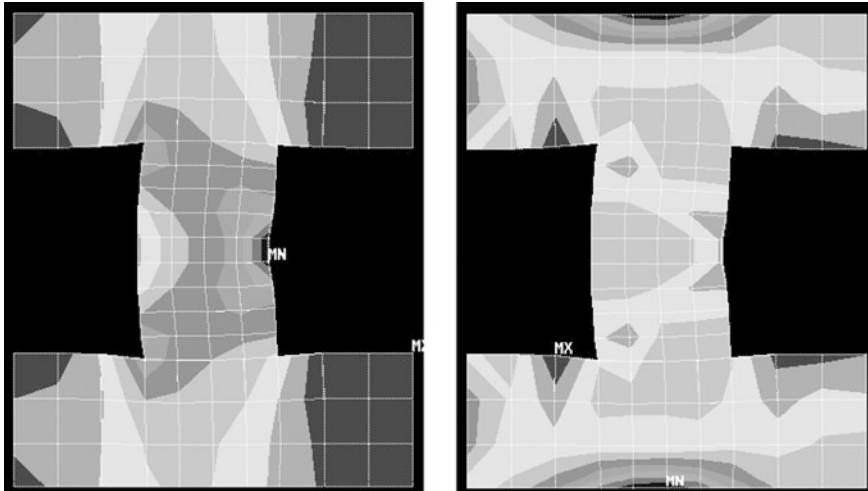
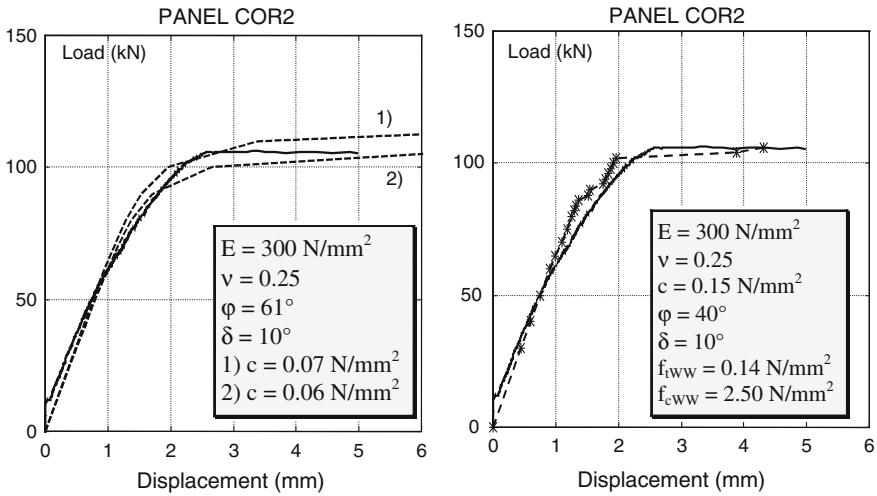


**Fig. 8** Numerical modelling of shear test on panel COR2: principal compressive stresses (*left*) and principal tensile stresses (*right*)

B in Pieve Fosciana. The model includes a considerable portion of the underlying masonry, the steel plates on the head and the system of vertical bars that originate the vertical load. Similar FE models were built to simulate the remaining shear and shear-compression tests. The numerical simulations were performed in two steps according to the experiments. In a first time the vertical pressure was applied, subsequently a monotonically increasing horizontal shear force was applied under load control using the Newton-Raphson method to solve the nonlinear equations. Figure 8 shows the maps of the principal stresses in an intermediate step of the analysis for the panel COR2. It is easy to recognize the formation of the two diagonal struts, in the map of the principal tensile stresses.

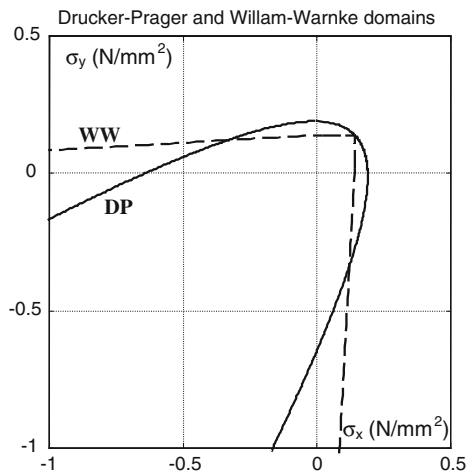
For the same panel, Fig. 9 shows a comparison between the numerical and the experimental results for both material models (plasticity only and plasticity and smeared crack models). In both cases it possible to observe a good approximation of the collapse load. The adoption of the smeared crack model in combination with the plasticity model allows to reproduce with good accuracy even the collapse displacement observed during the test (Fig. 9-right). On the contrary, the adoption of the elastic perfectly plastic model alone does not obviously reproduce the collapse displacement, since the panel behaves like an elastoplastic continuum with no limits to deformation.

Figure 10 shows, in the plane of the principal stresses (biaxial state), the particular combination of the DP and WW domains obtained for the numerical tuning of the test (Fig. 9-right). Values of the cohesion  $c = 0.15 \text{ N/mm}^2$  and  $\varphi = 40^\circ$  provide the masonry tensile strength  $f_{iDP} = 0.189 \text{ N/mm}^2$ , which is cutted by the choice of the parameter  $f_{iWW} = 0.14 \text{ N/mm}^2$  adopted in the WW model. The choice  $f_{cWW} = 2.5 \text{ N/mm}^2$ , greater than  $f_{cDP} = 0.643 \text{ N/mm}^2$  of the plasticity model, allows



**Fig. 9** Comparison between experimental and numerical results for shear test on panel COR2: plasticity model (*left*) and combined plasticity and failure models (*right*)

**Fig. 10** Intersection between the plasticity and the failure domains (panel COR2)



the correct simulation of the behaviour of the masonry in the mixed zone tension-compression. For the reproduction of the experimental results by using only the plasticity model, the friction parameter  $\varphi$  must be significantly higher than the correct choice for the combined models. The opposite happens for the cohesion  $c$ . Furthermore, the analysis highlighted the role of the dilatancy parameter  $\delta$  which identification has always provided values lower than the friction angle. This confirms the impossibility of using the associated flow law. The values of  $\beta_t$  and  $\beta_c$  were assumed equal to 0.25 and 0.75 for all the analyses.



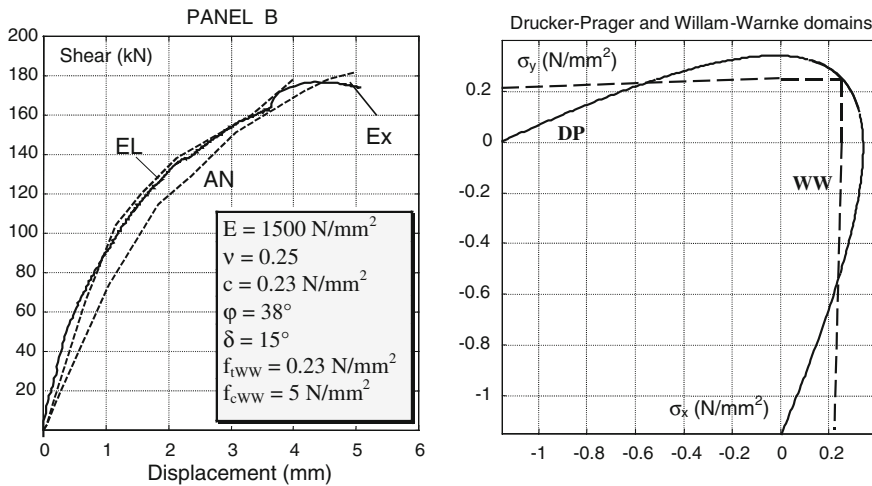


**Fig. 11** Comparison between experimental and numerical results for shear compression test on panel B (left) and intersection between the plasticity and the failure domains (right)

As an additional example, Fig. 11-left shows the result of the comparison of the curves shear-displacement in the middle cross-section obtained for the simulation of the test on panel B. The comparison refers to the model with both plasticity and cracking failure. The two curves (EL and AN) refer to different numerical modelling of the horizontal constraint of the head of the panel. The tuned combination of the models is reported in Fig. 11-right. Comparing the results of the numerical simulations on panels B and COR2 it is possible to observe a significantly higher values of the elastic modulus  $E$ , cohesion  $c$  and tensile strength for B. This is in agreement with the experimental evidence because the masonry texture of panel B was more compact than that of panel COR2.

A summary of the constitutive parameters which allowed a good reproduction of the experimental results in terms of shear-displacement curves is shown in Tables 3 and 4. In particular, Table 3 resumes the parameters identified for the DP model, whereas Table 4 reports the parameters identified for the DP model used together with the WW model. The tables report:

**Table 3** Identified model parameters (only plasticity model)

Panel ID	$E$ (N/mm <sup>2</sup> )	$\nu$	$c$ (N/mm <sup>2</sup> )	$\varphi$ (°)	$\delta$ (°)	$f_{cDP}$ (N/mm <sup>2</sup> )	$f_{tDP}$ (N/mm <sup>2</sup> )
COR2	300	0.25	0.065	61	10	0.503	0.049
COM	500	0.25	0.120	61	35	0.928	0.090
BEL	500	0.25	0.07	61	15	0.541	0.052
A	1500	0.25	0.28	40	15	1.201	0.353
B	1500	0.25	0.27	40	15	1.158	0.341

**Table 4** Identified model parameters (plasticity model combined with the smeared cracking and crushing model)

Panel ID	$c$ (N/mm <sup>2</sup> )	$\varphi$ (°)	$\delta$ (°)	$f_{cWW}$ (N/mm <sup>2</sup> )	$f_{iWW}$ (N/mm <sup>2</sup> )	$f_{cDP}$ (N/mm <sup>2</sup> )	$f_{iDP}$ (N/mm <sup>2</sup> )
COR2	0.150	40	10	2.5	0.14	0.643	0.189
COM	0.215	40	30	2.5	0.20	0.922	0.271
BEL	0.110	40	20	2.5	0.102	0.472	0.139
A	0.240	38	15	5.0	0.24	0.984	0.314
B	0.230	38	15	5.0	0.23	0.943	0.301

- the identified elastic parameters  $E$  and  $\nu$ ;
- the identified plastic parameters (DP):  $c$ ,  $\varphi$ ,  $\delta$  ( $f_{cDP}$  and  $f_{iDP}$ );
- the identified parameters of the cracking and crushing model (WW):  $f_{cWW}$ ,  $f_{iWW}$ .

According to the experimental results in terms of shear strength  $\tau_k$ , the panels can be divided into three classes (Chiostrini et al. 2000): (a) HS (high strength): panels A, B, COR3 and COM; (b) MS (medium strength): panels T1, T3, T4 and BEL; (c) LS (lower strength): panels T2, COR1, COR2 and E. HS corresponds to a good quality masonry; MS corresponds to a masonry with little internal voids, well filled by mortar and small dimension units; LS represents very poor assemblages of blocks and mortar, with many internal voids and facing walls weakly pinned. On the basis of such classification it is then possible to identify the ranges of variation of the parameters for the three classes of masonry (Table 5 for DP model and Table 6 for DP and WW models). Considering the difficulty to obtain specific results from monumental buildings, the reported values are typological reference data providing a reasonable estimation of these parameters (useful for the modelling of complex buildings whose walls textures are similar to those covered by the tests).

**Table 5** Variability of the parameters of the plasticity model

Masonry	$E$ (N/mm <sup>2</sup> )	$\nu$	$c$ (N/mm <sup>2</sup> )	$\varphi$ (°)	$\delta$ (°)
HS	500–1500	0.25	0.12–0.28	40–61	15–35
MS	350–500	0.25	0.07–0.09	38–61	12.5–15
LS	100–300	0.25	0.065	38–61	10–12.5

**Table 6** Variability of the parameters of the plasticity model combined with the failure criterion

Masonry	$c$ (N/mm <sup>2</sup> )	$\varphi$ (°)	$\delta$ (°)	$f_{cWW}$ (N/mm <sup>2</sup> )	$f_{iWW}$ (N/mm <sup>2</sup> )
HS	0.22–0.24	38–40	15–30	2.5–5.0	0.20–0.24
MS	0.11	38–40	12.5–20	2.5–3.0	0.10–0.11
LS	0.08–0.15	38–40	10–12.5	2.5–3.0	0.08–0.14

## 4 Illustrative Case Studies

In this section the model previously described is employed to analyse the seismic behaviour of two relevant masonry structures: a basilica-type church and a historic residential building. The two case studies demonstrate the careful use of nonlinear numerical analyses to address practical engineering problems in the field of seismic assessment of historic constructions.

### 4.1 *Masonry Church in Impruneta (Tuscany)*

As a first application, the analysis of the 14th century Basilica of Santa Maria all’Impruneta near Florence is discussed (Fig. 12). The plan view of the church (Fig. 13) shows the typical layout with a single nave and a polygonal apse separated by a triumphal arch. A pronaos, composed of five wide arches, and surmounted by rectangular windows, was built in 1634 and covers almost totally the old façade (Fig. 12).

#### 4.1.1 Geometry and Materials

An in situ survey of the church was made to obtain basic information on the geometry, the structural details and any irregularities. The investigation consisted in a geometrical relief, aimed at a check-up of wall-to-wall and wall-to-roof



**Fig. 12** Front view of the Basilica of Santa Maria all’Impruneta (Tuscany)

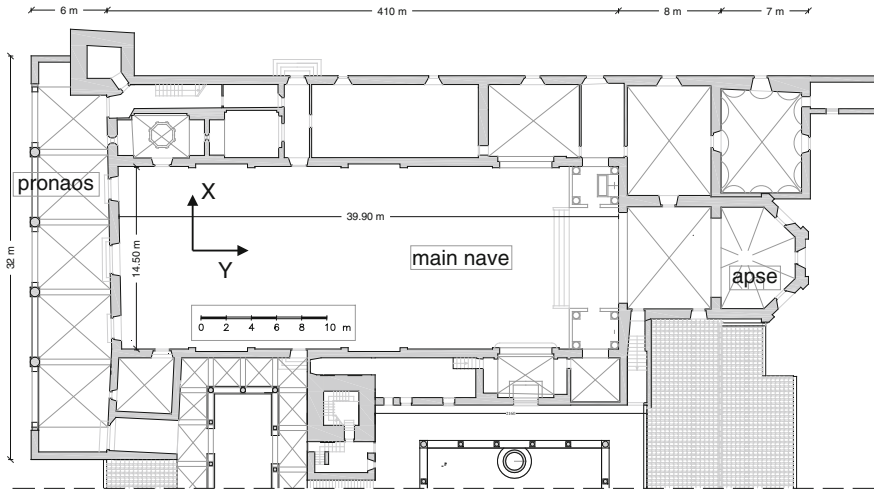


**Fig. 13** Plan layout of the Basilica of Santa Maria all'Impruneta

**Table 7** Elastic parameters of the main elements

	Nave	Apse	Columns
$E$ (N/mm <sup>2</sup> )	1400	1530	14,500
$\nu$	0.2	0.2	0.2
$\gamma$ (kg/m <sup>3</sup> )	1900	2000	2300

connections, and useful for the characterization of the masonry texture. This step was accompanied by a historical survey of the building to determine the original shape and eventually consider the church modifications over the centuries. Main dimensions of the nave are the following: maximum length of about 39.90 m, maximum width of 14.50 m and walls with height of about 15.0 m. The thickness of the masonry walls ranges between 0.70 m (nave walls) and 0.80 m (apse walls) and the nave roof is made of a timber structure. The walls are single-leaf, with several types of masonry weaving, differing both in materials (stones, bricks, etc.) and textures (*opus incertum*, *opus mixtum*, etc.). However, despite these differences, the construction is mostly made of irregular sandstone masonry with thick lime mortar joints. Local stones are also used for windows, apse and doors jambs. For the mechanical characterization of the elastic properties of the masonry the Italian Recommendations were employed (OPCM 2003; NTC 2008), assuming the conservative values for historic masonry (Table 7,  $\gamma$  denotes the specific weight).

#### 4.1.2 Numerical Modelling

The structural behaviour of the church was analysed through a complete 3D analysis using the FE technique and the macro-modelling strategy. This

computational strategy, as reported above, is convenient for large scale models. Other strategies, suitable mainly for small size models, rely on micro-modelling approaches where units and mortar are modelled separately. An additional comprehensive recent discussion on these aspects is reported in Berto et al. (2005), Adam et al. (2010), Lourenço and Pina-Henriques (2006). The model of the whole *fabrica* was built by the code ANSYS (1998) to accurately reproduce the geometry of the structure, focusing on the variations in the wall thickness, on the geometrical and structural irregularities and on the wall connections.

Masonry walls were modelled by means of *Solid65* elements (Fig. 1); *Shell63* elements (two-dimensional isoparametric elements with four nodes) were used to model the main vault and the annexed buildings; *Beam44* elements (one-dimensional isoparametric elements with two nodes) were employed for modelling the queen truss on the timber roof of the main nave. The major openings in the building were reproduced, and the nonlinear analyses were performed assuming a rigid ground foundation (fixed base model). The final 3D model (Fig. 14) consists of 27,779 nodes, 76,895 3D *Solid65* elements, 1751 2D *Shell63* elements and 547 1D *Beam44* elements, that correspond to 81,021 degrees of freedom. The nonlinear behaviour of the masonry was reproduced by the proper combinations of the DP model with the WW failure surface. The conservative values for historic masonry were assumed, taking into account the Italian

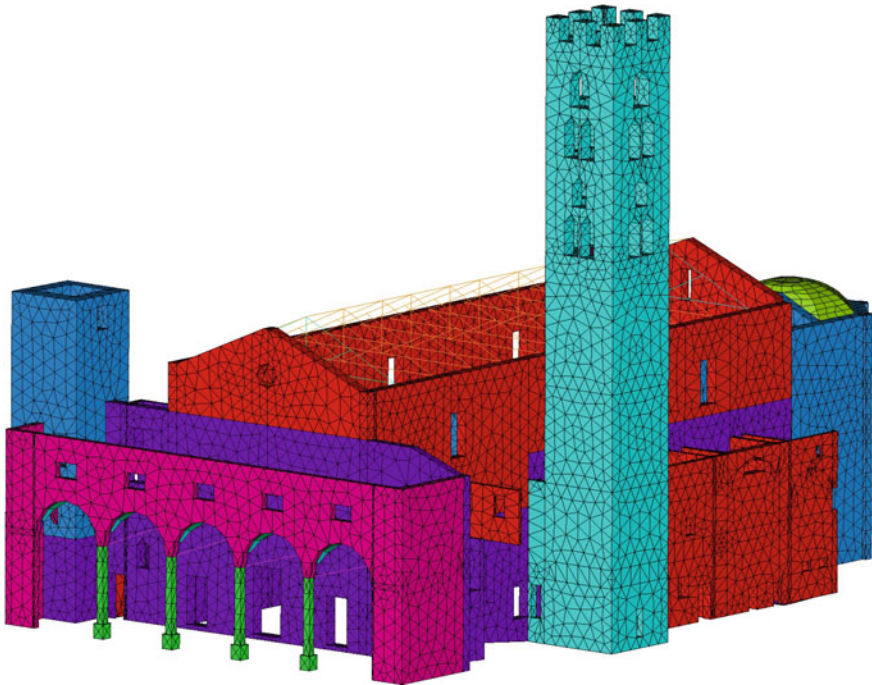


**Fig. 14** Finite element model of the Basilica

**Table 8** Drucker-Prager yield criterion (main elements)

	Nave	Apse	Columns
$c$ (N/mm <sup>2</sup> )	0.1	0.1	0.5
$\varphi$ (°)	38	38	38
$\delta$ (°)	15	15	15

**Table 9** Willam-Warnke failure surface (main elements)

	Nave	Apse	Columns
$f_{cww}$ (N/mm <sup>2</sup> )	7.5	8.5	40
$f_{tww}$ (N/mm <sup>2</sup> )	0.15	0.15	3.5
$\beta_c$	0.75	0.75	0.75
$\beta_t$	0.15	0.15	0.15

Recommendations (OPCM 2003; NTC 2008) and the identification reported in the previous section. Tables 8 and 9 report the selected parameters of the model with respect to the main elements of the Basilica.

### 4.1.3 Static Analysis

Firstly, the static behaviour of the Basilica was analysed under the vertical loads deriving from the own weight of the walls and from the roof loads (1.1 kN/m<sup>2</sup> according to the Italian standards). The overall structure was analysed in the nonlinear range through the complete 3D model with the aim to obtain valuable information on the global behaviour and on the interaction among the single elementary parts. Finally, it was possible to identify the weak points of potential failure in the church. Results of the static analysis in terms of vertical stresses are reported in Figs. 15 and 16. In general, the stress state induced on the church by the static vertical loads is quite moderate. The average compressive stress on the nave walls is about 0.6 N/mm<sup>2</sup>. Small values of tensile stresses appear on the top surface of the nave walls, due to the timber roof loads. Mainly, this is a local numerical effect depending on the punctual connection between the beams and the solid elements.

The maximum value of the compression is reached in the columns of the pronaos (Fig. 16) where the compressive stresses reach values of about 2.0–2.5 N/mm<sup>2</sup>. Even if this stress level seems high when compared with the medium value of the compressive stresses it is lower than the crushing limit of the sandstone material of the columns. Anyway, among the various structural elements that compose the church, these columns (actually reinforced by steel collars) are the critical elements.

Results of the analysis substantially confirm that the church is adequate to withstand the vertical loads. This is a quite common result for this typology of buildings designed by skilled manufacturers to attempt very slender schemes. Results in terms of displacement show that the maximum value is reached close to the triumphal arch between the nave and the apse.

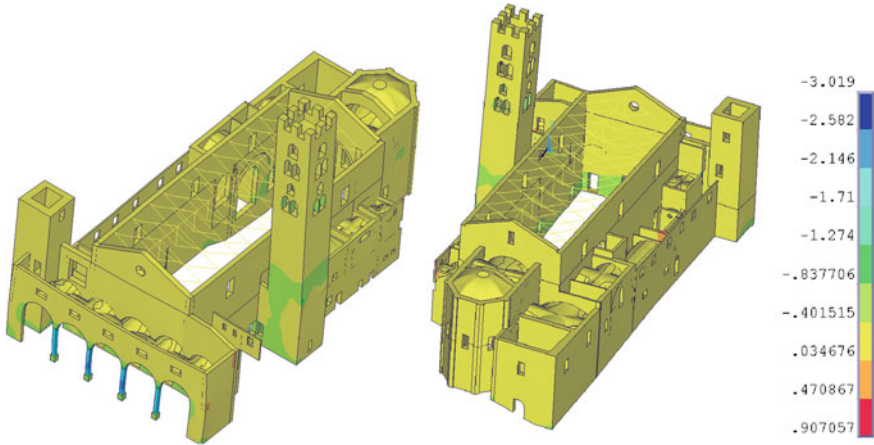


**Fig. 15** Vertical stresses  $\sigma_z$  (N/mm<sup>2</sup>): global view

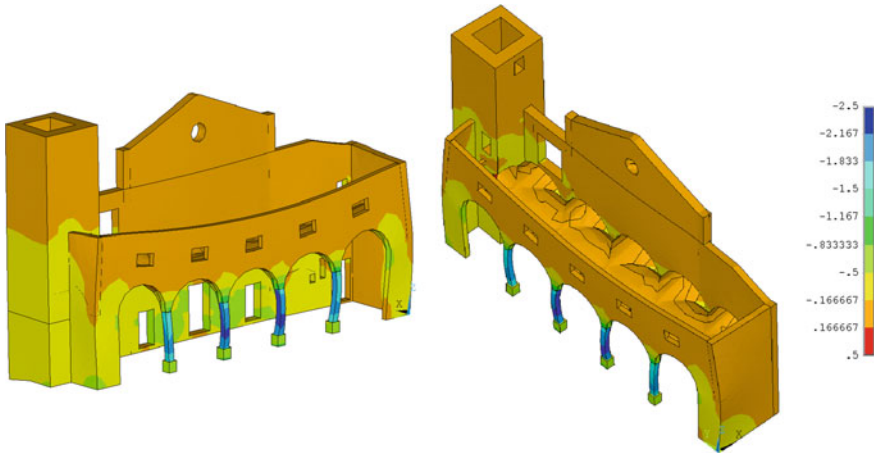


**Fig. 16** Vertical stresses  $\sigma_z$  (N/mm<sup>2</sup>): façade wall detail

#### 4.1.4 Modal Analysis

The 3D model was also used to assess the modal behaviour of the Basilica. The first 100 modal shapes of the church were evaluated to assure that the total effective modal mass of the model was at least 90 % of the actual mass. The outcome was that 90 % of the total mass was accounted for by using the first 87 modes. Effective and cumulative masses of the first 10 global vibration modes in the transversal, longitudinal and vertical direction of the church are reported in Table 10. The first modal shape of the church involves the translation in the weakest transversal direction of the main nave, with significant out-of-plane deformation of the



**Table 10** Church modal effective masses for transversal, longitudinal and vertical direction

Mode $n$ °	Period (s)	X direction (transversal)		Y direction (longitudinal)		Z direction (vertical)	
		$M_{eff}$ (%)	$\Sigma M_{eff}$ (%)	$M_{eff}$ (%)	$\Sigma M_{eff}$ (%)	$M_{eff}$ (%)	$\Sigma M_{eff}$ (%)
1	0.585	14.11	23.95	0.03	10.58	0.00	0.24
2	0.480	0.01	23.96	2.92	13.50	0.00	0.24
3	0.404	0.72	24.68	0.02	13.53	0.00	0.25
4	0.385	1.28	25.96	8.62	22.15	0.00	0.25
5	0.334	1.13	27.68	0.93	27.57	0.01	0.36
6	0.298	18.38	46.06	0.19	27.76	0.26	0.62
7	0.297	5.31	51.37	0.02	27.78	2.86	3.48
8	0.289	0.67	55.22	0.73	28.53	0.00	8.43
9	0.261	0.00	55.22	6.10	34.64	0.28	8.71
10	0.242	5.66	62.87	0.29	35.11	0.12	8.88

orthogonal elements (Fig. 17). The higher modal shapes of the church are a combination of transversal vibration modes and torsional modes. The distribution of the modal shapes demonstrates that the church, though characterised by stiff structural elements on the perimeter, displays low transversal and torsional stiffnesses, with significant out-of-plane deformations of the elements. Furthermore, the deformed plan configuration confirms that the seismic loads acting along either longitudinal or transversal direction involve remarkable out-of-plane deformations of the orthogonal structural elements.

#### 4.1.5 Seismic Vulnerability

The analysis of the seismic behaviour was performed by means of a pushover analysis (Falasco et al. 2006; Kim and D'Amore 1999). Monotonically increasing horizontal loads were applied under conditions of constant gravity loads. Based on this analysis method, the effects of the seismic loads were evaluated by applying two systems of horizontal forces perpendicular to one another. These forces, not acting simultaneously, were evaluated taking into account two load distributions. The first distribution was directly proportional to the masses of the church (uniform); the second distribution was proportional to the product of the masses by the displacements of the corresponding first modal shape. These two load distributions could be considered as representative of two limit states for the capacity of the building. The first distribution assumes that the horizontal loads are constant with respect to the height. This means that the displacements of the lower level of the church are overestimated, while the opposite happens for the displacement of the top level. On the contrary, the second distribution overestimates the displacement on the top level. Is it noteworthy to point out that a conventional pushover was performed in the study, i.e. loads applied on the building didn't change with the



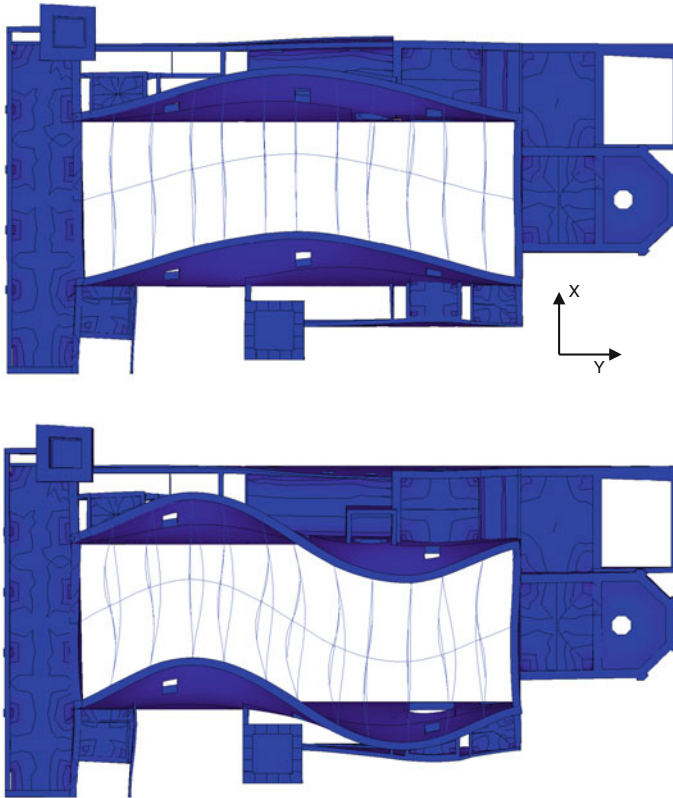


**Fig. 17** First two transversal modal shapes of the church:  $T_1 = 0.585$  s ( $f_1 = 1.704$  Hz) and  $T_3 = 0.404$  s ( $f_3 = 2.475$  Hz)

progressive degradation occurring during the loading process (Antoniou and Pinho 2004; Chopra and Goel 2004).

The critical load distribution for the Basilica corresponds to the case of the load acting in the transversal direction, perpendicular to main nave. So, results are mainly next detailed with respect to this case. This behaviour was expected due to the fact that the transversal direction of the church involves remarkable out-of-plane deformations of the orthogonal structural elements. Figure 18 reports the displacements in the transversal direction at the end of the analysis and Fig. 19 reports the corresponding cracking pattern; it involves almost all the nave walls, together with the orthogonal ones. The cracking behaviour, compared with the overall deformative behaviour, shows a poor stiffness of the church in the transversal direction. Figures 20 and 21 report, respectively, the deformative behaviour and the cracking pattern that arises in the church with respect to the load acting in the longitudinal direction. The structural elements more vulnerable are the pronaos and the façade. The analyses stop at a level of the horizontal load of about the 18–20 % of the overall weight of the church.

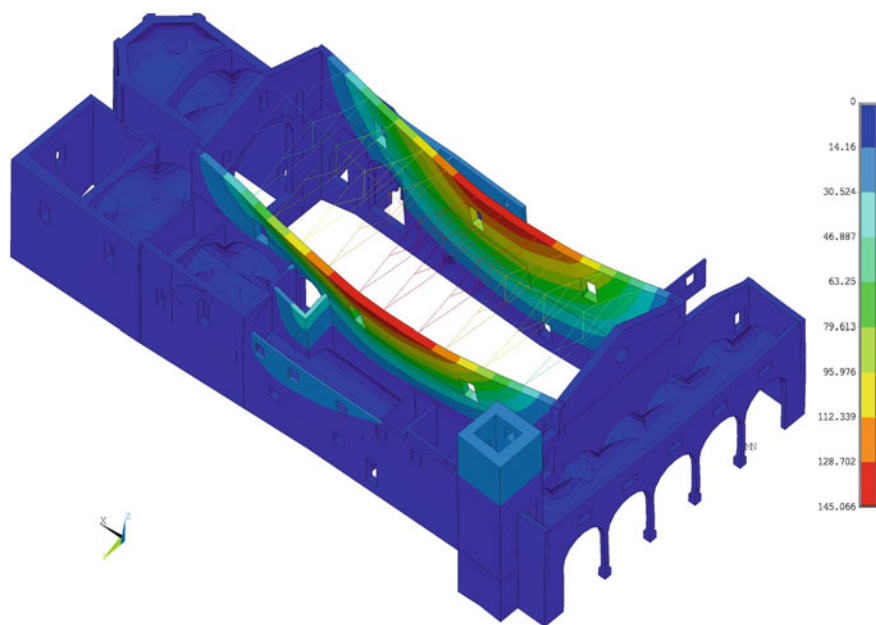


**Fig. 18** Pushover analysis with uniform horizontal loads in the transversal direction: displacement (mm)

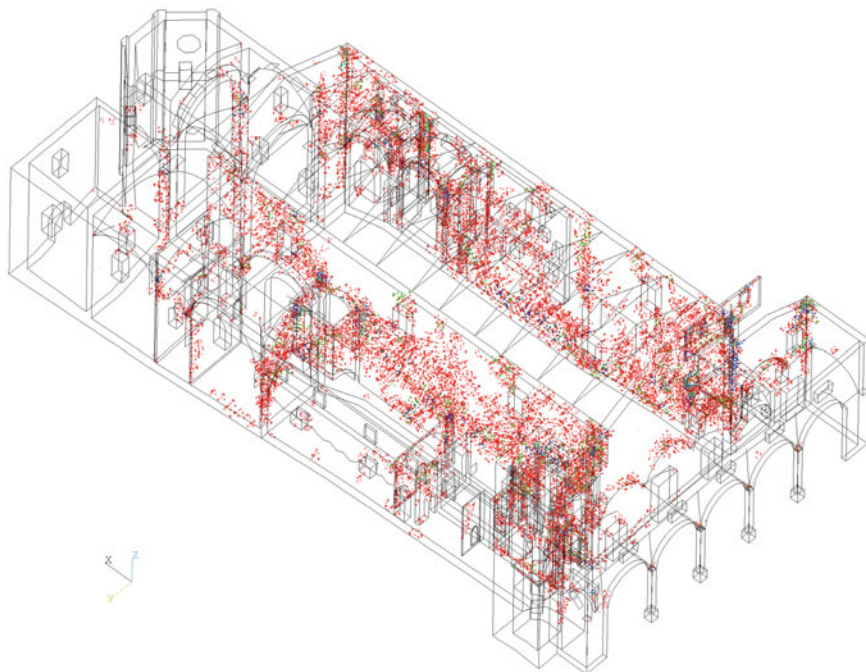


**Fig. 19** Pushover analysis with uniform horizontal loads in the transversal direction: cracking pattern

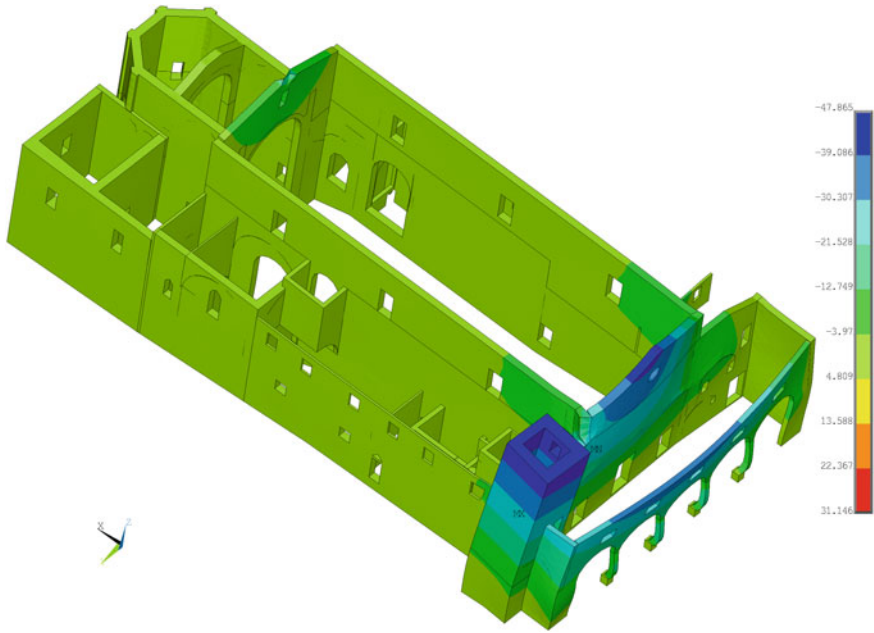


**Fig. 20** Pushover analysis with uniform horizontal loads in the longitudinal direction: displacement (mm)

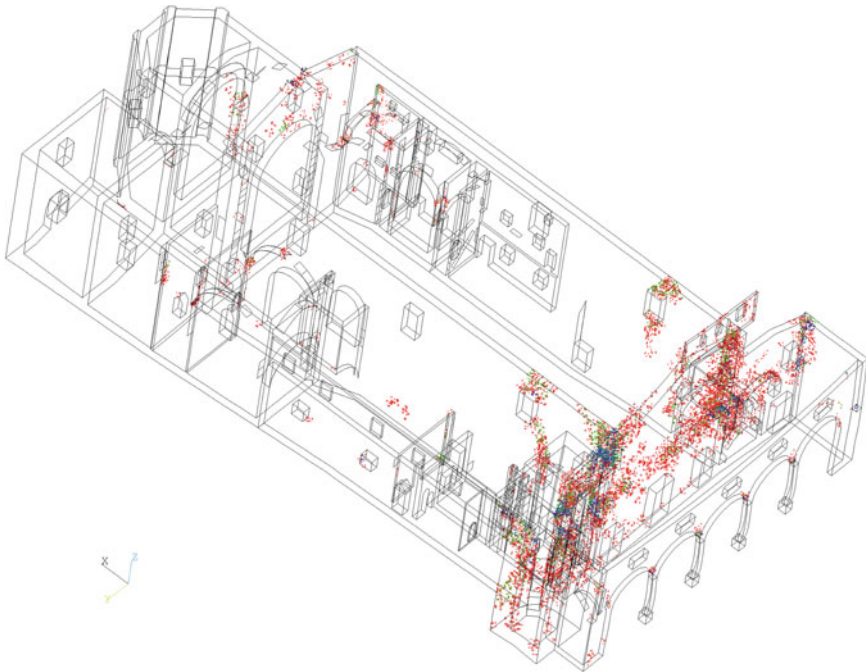


**Fig. 21** Pushover analysis with uniform horizontal loads in the longitudinal direction: cracking pattern

The cracking pattern suggests the mechanism to be considered in the limit state analysis and offers an indication on the potential strengthening design (Lourenço and Oliveira 2007). The critical elements of the church are the lateral walls of the nave, which require to increase their out-of-plane strength. In order to generate a box-behaviour a global reinforcement of the queen roof can be performed by means of a system of horizontal counterbracing to be inserted between the extrados of the timber roof and the tile covering. The steel counterbracing, directly connected to the wooden beams of the queen roof, could be designed to create a top rigid floor that may ensure a box-behaviour of the nave. A local steel reinforcement of the connections between the timber structure and the masonry walls needs to be provided to avoid local failure. Additional local reinforcements may be inserted along the Basilica, in particular a steel tie could be placed along the apse perimeter.

## 4.2 *Masonry Building in Fivizzano (Lunigiana)*

The object of the second application is a residential building located in the historic city centre of Fivizzano in Lunigiana (Fig. 22). The building was damaged by an earthquake in October 1995 (4.7 magnitude on the Richter Scale), and subsequently retrofitted in December 1997. The building is an illustrative example, since it is representative of many typical masonry buildings of Central Italy, with architectural and structural features (as well as the seismic damages suffered during the earthquake) similar to those found in many other buildings. The moderate damages caused by the earthquake suggested the employment of traditional retrofitting techniques such as the insertion of steel chains at several levels. The numerical analyses aimed at assessing the effectiveness of the retrofitting by comparing the seismic behaviour of the building after and before the insertion of the steel chains.

### 4.2.1 Description

The construction is composed of two adjacent buildings with different heights, joined by a common wall (Fig. 22). Over time, the original structure of the building, that dates back to the eighteenth century, has been undergoing continuous structural and architectural changes, especially after the 1920 and 1967 earthquakes which led to the current configuration. As a part of the last restructuring in 1967, an additional floor was built with the creation of two units. Today the building has an irregular shape with two levels above ground and one basement.

The masonry walls are made of rubble stone masonry (an example of the chaotic texture is reported in Fig. 23) with the exception of the corners, where regular-shaped well-connected stones are visible. On the first floor there are two



**Fig. 22** Front view (South-West)

**Fig. 23** View of the masonry texture



heads brick walls, on the second floor a concrete wall was found, probably introduced during the last renovation in 1967. Lintels over doors and windows are made of hewn stone. The thickness of the stone walls varies from 0.55 to 1.00 m. Different types of floors are present. On the first floor there are stone vaults, the other levels are made of steel profiles (NP 140) and hollow flat blocks without concrete. The roof is made with wooden beams simply leaned on the perimeter walls. In the South-East portion of the building the roof is made by means of a reinforced concrete (RC) slab supported by rectangular concrete beams still leaned on the perimeter walls. Despite the last restructuring of the building dates back to 1967, there are no perimeter concrete beams.

During the 1995 earthquake the building was damaged and a series of cracks with a thickness of a few mm, formed on the first and the ground floor walls. Cracks passing through the wall thickness arose on North-West façade and in some internal walls. The seismic strengthening of the building, which ended in December 1997,

was made through the introduction of steel chains at the level of the first and the second floor, and in correspondence of the first floor vault (Fig. 24).

The retrofitting was limited to the North-West area of the building, the most damaged during the 1995 earthquake and circular steel chains with diameter ranging from 18 to 24 mm were used. It is worth noting that the position and the number of the steel chains was decided without any provisional design, being selected only based on the building damage.

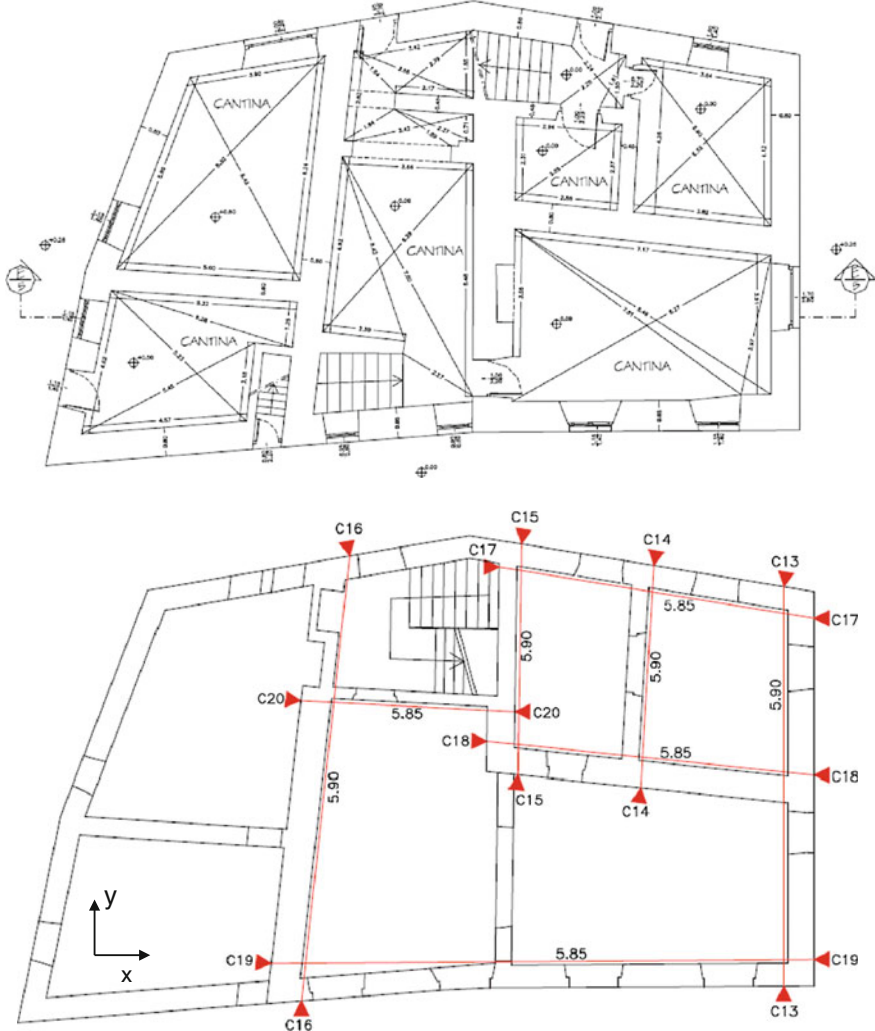


Fig. 24 First floor layout (up) and position of the steel chains (down)



### 4.2.2 Numerical Modelling

To analyse the seismic behaviour of the building before and after the retrofitting, a numerical model of the construction was built using the commercial code ANSY. The model includes the following structural elements: the masonry walls, the structural part of the stone vaults, the steel floors, the wooden cover roof, the reinforced concrete slab and the concrete wall (Fig. 25). Stairs were not considered in the model, since most of these are cantilever stairs without structural continuity with the confining walls (stairs were assumed as additional masses). The numerical model of the building before the retrofitting with steel chains comprised a total of 8404 elements, corresponding to 41,676 degrees of freedom (Fig. 25). In particular, the masonry walls were modelled by the elements *Solid65*, the steel floors by the elements *Beam8* and the masses by the elements *Mass21*. Finally, the RC slab was modelled through the elements *Shell63*.

The masonry nonlinear behaviour was defined by the combination of the DP plasticity model with the WW failure model. The mechanical characteristics of the in situ masonry were defined assuming the ones corresponding to the typology HS of Sect. 3 (Table 11). The elastic properties of the main elements are resumed in Table 12.

A preliminary static analysis under vertical dead and live loads was performed according to the Italian Recommendations in force at the time of retrofitting (1997) (DM96 1996). The maximum compression in the masonry at the ground level was found to be about  $0.697 \text{ N/mm}^2$ . The modal analysis provided the following results (Fig. 26). The first modal shape ( $f_1 = 5.34 \text{ Hz}$ ) involves the translation in the  $Y$  direction and mainly concern the bending deformation of the second floor. The second modal shape ( $f_2 = 6.74 \text{ Hz}$ ) is a torsional mode and again mainly involves deformations of the second floor. The third modal shape ( $f_3 = 7.49 \text{ Hz}$ ) is another torsional mode similar to the previous mode. Considering the first 20 modes, they activated more than 90 % of the total mass in the  $X$  and  $Y$  directions, only 59.7 % in the vertical direction.

### 4.2.3 Assessment of the Past Retrofitting

The structural behaviour of the building with and without the steel chains was analysed performing nonlinear seismic analyses, to assess the effectiveness of the post-earthquake strengthening. Two distributions of horizontal forces were preliminary considered. The first seismic equivalent load distribution was assumed according to the Italian Recommendations in force at the time of retrofitting (DM96 1996). The second load distribution was considered according to Eurocode 8 (1996).

The two codes differ in the manner in which the seismic actions are evaluated. The equivalent static analysis proposed by the DM96 (1996) considers a set of horizontal loads along the height of the building according to the distribution of the masses multiplied by the heights. The simplified dynamic analysis proposed by the

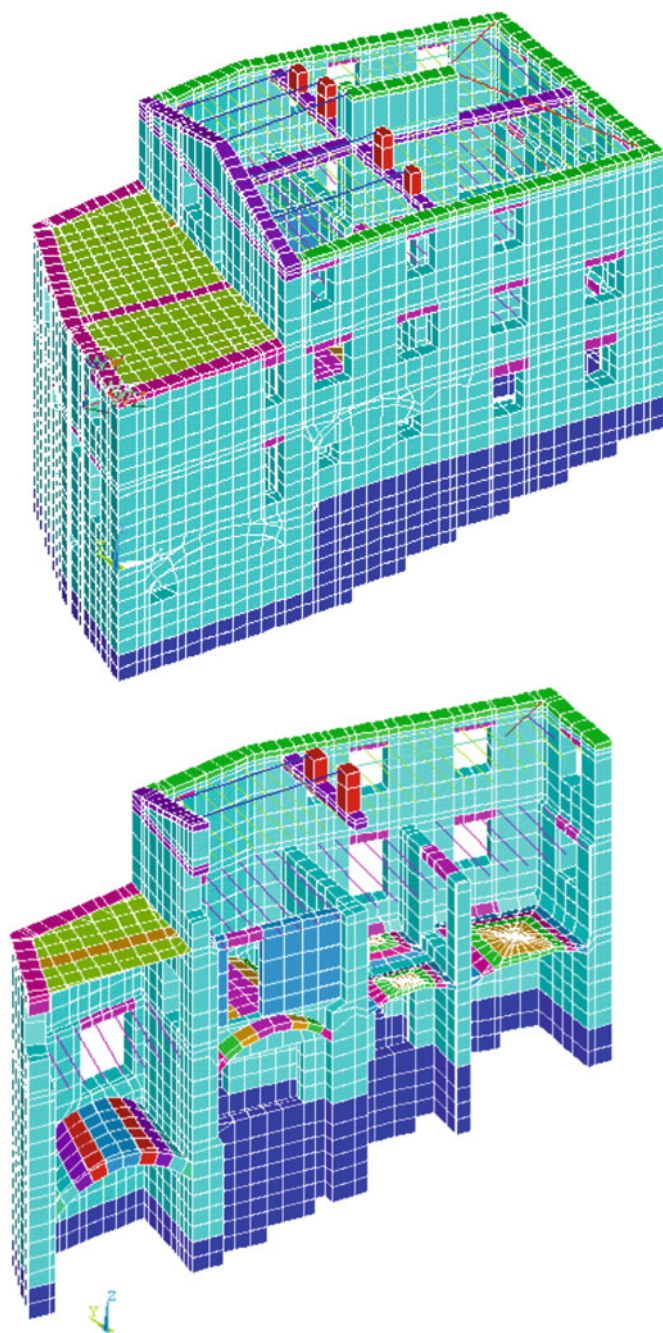


**Fig. 25** Finite element model of the building in Fivizzano (Lunigiana)



**Table 11** DP and WW model parameters

$c$ (N/mm <sup>2</sup> )	$\varphi$ (°)	$\delta$ (°)	$f_{cWW}$ (N/mm <sup>2</sup> )	$f_{iWW}$ (N/mm <sup>2</sup> )	$\beta_c$	$\beta_t$
0.24	38	15	6.0	0.25	0.75	0.15

**Table 12** Elastic parameters (main elements)

	Masonry walls	Stone jambs	Reinforced concrete	Wooden beams
$E$ (N/mm <sup>2</sup> )	1800	3000	30,000	11,500
$\nu$	0.2	0.3	0.16	0.25
$\gamma$ (kg/m <sup>3</sup> )	2200	2200	2500	600

Eurocode 8 (1996) adopts instead a distribution of seismic loads based on the displacement of a modal shape, without any assumptions about the shape of this mode. The first mode of the building in Fivizzano is significantly different from the linear shape along the height assumed in DM96 (1996), which is therefore not fully reliable. This fact was indirectly confirmed by a preliminary analysis where quite good agreement with the state of the 1995 damage was obtained only with the simplified dynamic analysis performed using the modal load distribution proposed by the Eurocode 8 (1996). Therefore, the comparative nonlinear analyses were performed assuming the seismic forces distribution proposed by the Eurocode 8 (1996). The procedure consisted of two phases: the first phase in which vertical loads were applied (dead and live loads) and the second phase, divided into sub steps, in which the equivalent horizontal seismic actions were applied.

#### 4.2.4 Nonlinear Analyses

In the second phase, the analysis of the building before retrofitting was stopped in the step corresponding to a value of the seismic loading of about 70 % of the full load (evaluated assuming a behaviour factor  $q = 1.5$ , a damping ratio  $\xi = 0.08$ , a peak ground acceleration  $a_g/g = 0.25$ , and a soil type A). The analysis of the results in terms of cracked area showed that the damage was localized at the top of the walls W1 and W3 (Fig. 27) with out-of-plane deformation. Other damages were observed in the wall W6, in the zone above the door and under the second floor window (Figs. 27 and 28).

To evaluate the improvement obtained with the insertion of the steel chains, three additional nonlinear analyses with different values of pretension of the steel chains were performed: pretension  $\sigma_f$  equal to 70 N/mm<sup>2</sup> (Case 1), 100 N/mm<sup>2</sup> (Case 2) and 120 N/mm<sup>2</sup> (Case 3). Higher values were not considered to avoid local damages on the masonry. The chains were modelled with two-nodes linear elements (*Link8*), and the coupling of the link with the masonry (the steel plate) was modelled through shell elements (*Shell63*), to allow for a local distribution of the stresses. The failure modes predicted by the retrofitted model remain basically the

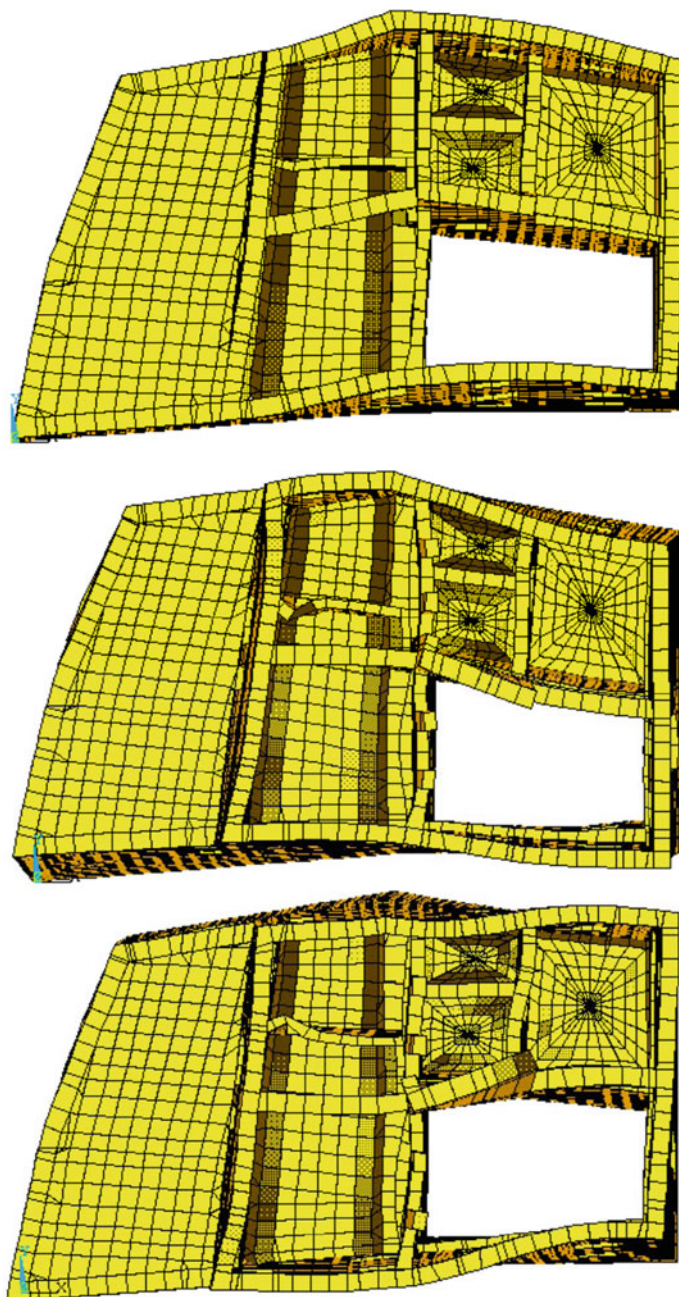


**Fig. 26** First three modal shapes of the building:  $T_1 = 0.187$  s ( $f_1 = 5.34$  Hz),  $T_2 = 0.148$  s ( $f_2 = 6.74$  Hz) and  $T_3 = 0.133$  s ( $f_3 = 7.49$  Hz)

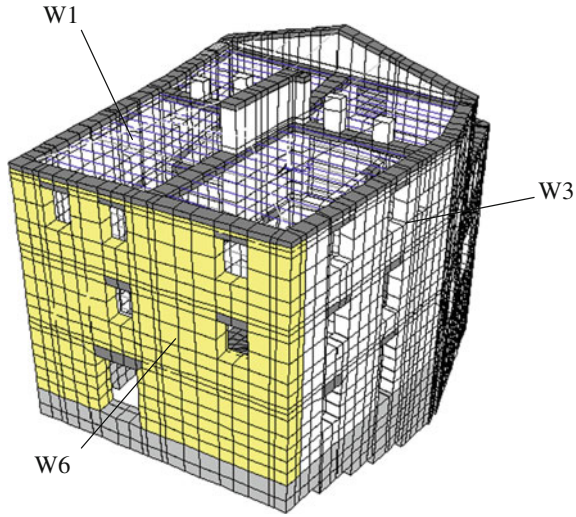


Fig. 27 Designation of the main walls

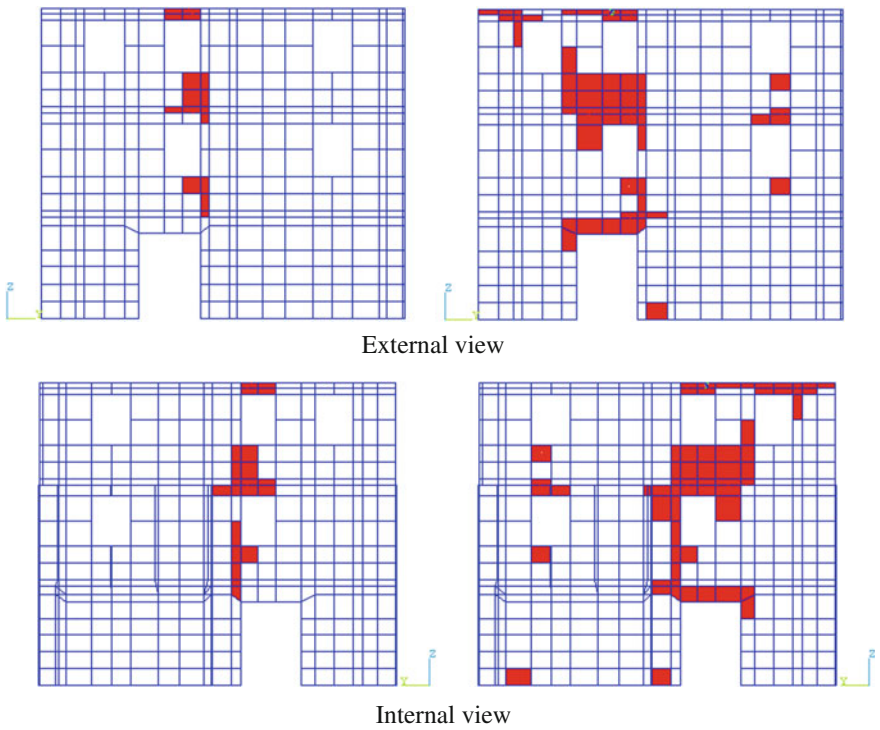


Fig. 28 Evolution of the cracking pattern on the wall W6: intermediate step of the analysis (left) and collapse configuration (right) (red denotes the cracked and/or the crushed elements)

**Table 13** Benefits of the different levels of strengthening retrofitting

Nonlinear analysis	Chain pretension $\sigma_f$ (N/mm <sup>2</sup> )	Collapse loads (% of the seismic load)	Increment (%)
Without steel chains	0	70	/
Case 1	70	72	2.86
Case 2	100	76	9.29
Case 3	120	82	17.14

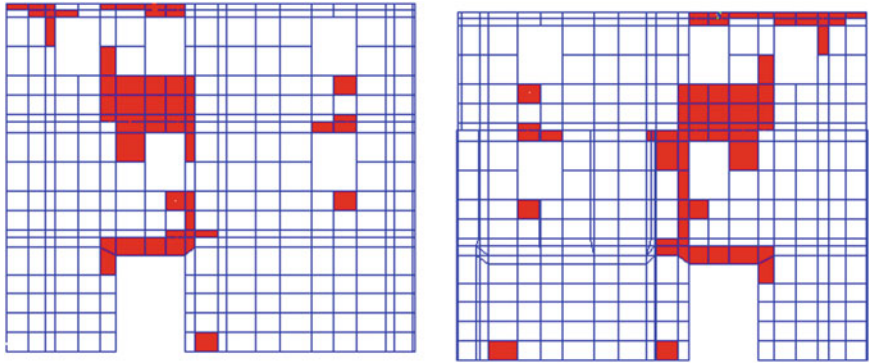
same, but an increment of the collapse load was observed (Table 13). The table reports also the improvement obtained increasing the stress in the chains. This benefit varies from about 2.8 % in the first case up to 17 % in the last case. The benefit obtained by the insertion of the chains is shown in Fig. 29 that reports the distribution of the cracked areas at collapse in the wall W6.

## 5 Conclusions

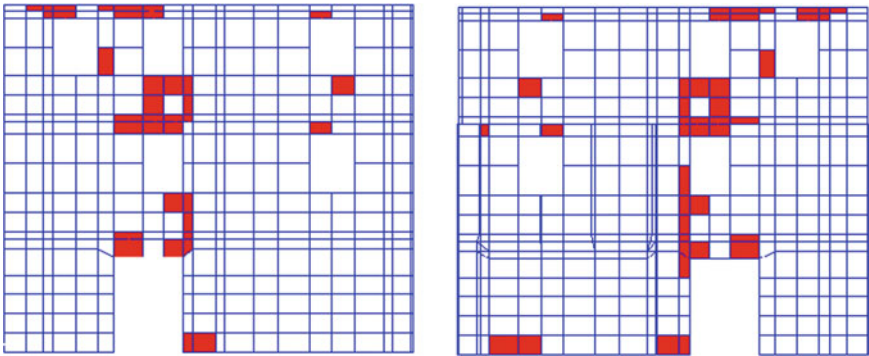
Modern societies consider preservation of built heritage, and passing it to future generations, a major issue (Fioravanti and Mecca 2011) since it contributes to consolidating a collective memory that creates a sense of belonging in citizens. In addition, from an economic point of view, and especially in contexts where tourism is becoming a major industry, accessibility to cultural heritage significantly contributes to the community's development (Bowitz and Ibenholt 2009).

Conservation of heritage buildings is an historical, cultural and engineering process (ICOMOS 2001) where safety evaluation should be correlated with proper principles of structural conservation (conserve as found, minimal intervention, like-for-like repairs, repairs reversible, etc.) according to a multidisciplinary and multicultural approach. From the specific engineering perspective, preservation calls for an interconnected series of operations aimed at obtaining a satisfactory broad-spectrum knowledge level of the building, where traditional in situ investigations must be performed in parallel with advanced numerical analyses such as the one discussed in the chapter. In fact, a clear understanding of the actual structural behaviour based on sophisticated numerical tools is an effective item of the path of knowledge that is needed for the proper design of a reliable strengthening that prevents invasive and inappropriate retrofitting.

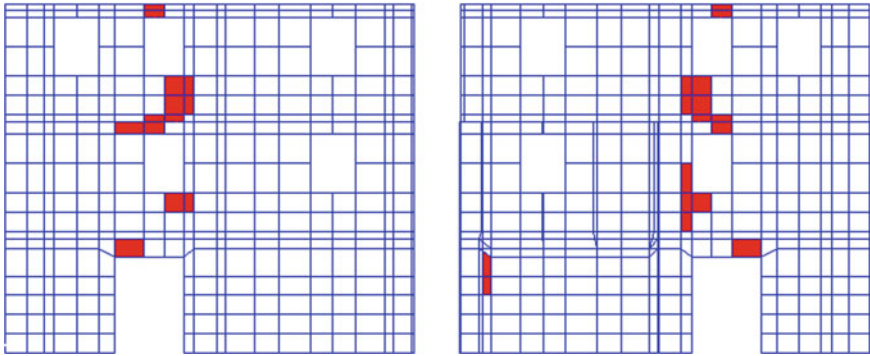
With this focus the chapter discussed on the application of the finite element technique for seismic vulnerability assessment of historic masonry buildings. In a first part, two numerical models employed to reproduce the nonlinear masonry behaviour were explained, together with the identification of the required parameters. The models were a plasticity model and a combined plasticity and smeared cracking/crushing model. The tuning of the required parameters was performed based on the numerical reproduction of in situ experimental tests. So, a set of values



Case 1



Case 2



Case 3

**Fig. 29** Collapse configuration on wall W6: external view (*left*); internal view (*right*) (*red* denotes the cracked and/or the crushed elements)

were proposed for three typologies of historic masonries characterized by high, medium and low strength. Subsequently, in a second part, the models were employed to analyse the seismic behaviour of a monumental masonry church and a residential masonry building.

According to the presented numerical modelling, the chapter indicates that advanced computational analyses can significantly contribute to the understanding of the actual behaviour of historic buildings under seismic loading. Such knowledge, in its turn, allows to correctly design the strengthening interventions required for the safety and accessibility of the building.

## References

- Adam, J. M., Brencich, A., Hughes, T., & Jefferson, T. (2010). Micromodelling of eccentrically loaded brickwork: Study of masonry wallets. *Engineering Structures*, 32(5), 1244–1251.
- Adam, J. M., Ivorra, S., Pallarés, F. J., Giménez, E., & Calderón, P. A. (2009). Axially loaded RC columns strengthened by steel caging. Finite element modelling. *Construction and Building Materials*, 23(6), 2265–2276.
- ANSYS Inc. (1998). *ANSYS manual*. USA: Southpoint.
- Antoniou, S., & Pinho, R. (2004). Advantages and limitations of adaptive and non adaptive force-based pushover procedures. *Journal of Earthquake Engineering*, 8(4), 497–522.
- Bartoli, G., & Betti, M. (2013). Cappella dei Principi in Firenze, Italy: Experimental analyses and numerical modeling for the investigation of a local failure. *ASCE's Journal of Performance of Constructed Facilities*, 27(1), 4–26.
- Berto, L., Saetta, A., Scotta, R., & Vitaliani, R. (2005). Failure mechanism prism loaded in axial compression: Computational aspects. *Materials and Structures*, 38, 249–256.
- Betti, M., Bartoli, G., & Orlando, M. (2010). Evaluation study on structural fault of a Renaissance Italian Palace. *Engineering Structures*, 32(7), 1801–1813.
- Betti, M., & Vignoli, A. (2008). Modelling and analysis of a Romanesque church under earthquake loading: Assessment of seismic resistance. *Engineering Structures*, 30(2), 352–367.
- Binda, L., Saisi, A., & Tiraboschi, C. (2000). Investigation procedures for the diagnosis of historic masonries. *Construction and Building Materials*, 14, 199–233.
- Borri, A., Corradi, M., & Vignoli, A. (2000). Il comportamento strutturale della muratura nelle zone terremotate dell'Umbria: alcune sperimentazioni. *Ingegneria Sismica*, XVII(3), 23–33. (in Italian).
- Bowitz, E., & Ibenholt, K. (2009). Economic impacts of cultural heritage—Research and perspectives. *Journal of Cultural Heritage*, 10(1), 1–8.
- Brandonisio, G., Lucibello, G., Mele, E., & De Luca, A. (2013). Damage and performance evaluation of masonry churches in the 2009 L'Aquila earthquake. *Engineering Failure Analysis*, 34, 693–714.
- Carpinteri, A., Invernizzi, S., & Lacidogna, G. (2005). In situ damage assessment and nonlinear modelling of a historical masonry tower. *Engineering Structures*, 27, 387–395.
- Ceci, A. M., Contento, A., Fanale, L., Galeota, D., Gattulli, V., Lepidi, M., & Potenza, F. (2013). Structural performance of the historic and modern buildings of the University of L'Aquila during the seismic events of April 2009. *Engineering Structures*, 32(7), 1899–1924.
- Cerioni, R., Brighenti, R., & Donida, G. (1995). Use of incompatible displacement modes in a finite element model to analyze the dynamic behavior of unreinforced masonry panels. *Computers & Structures*, 57(1), 47–57.



- Chiostrini, S., Galano, L., & Vignoli, A. (1998). In situ tests and numerical simulations on structural behaviour of ancient masonry. In *Proceedings of Monument-98, Workshop on Seismic Performance of Monuments, Lisbon*.
- Chiostrini, S., Galano, L., & Vignoli, A. (2000). On the determination of strength of ancient masonry walls via experimental tests. In *Proceedings of 12 WCEE, Auckland, New Zealand, January 30–February 4, 2000*.
- Chiostrini, S., Galano, L., & Vignoli, A. (2003). In situ shear and compression tests in ancient stone masonry walls of Tuscany, Italy. *ASTM Journal of Testing and Evaluation*, 31(4), 289–304.
- Chiostrini, S., & Vignoli, A. (1992). An experimental research program on the behavior of stone masonry structures. *ASTM Journal of Testing and Evaluation*, 20(3), 190–206.
- Chiostrini, S., & Vignoli, A. (1994). In-situ determination of the strength properties of masonry walls by destructive shear and compression tests. *Masonry International*, 7(3), 87–96.
- Chopra, A. K., & Goel, R. K. (2004). A modal pushover analysis procedure to estimate seismic demands for unsymmetric-plan buildings. *Earthquake Engineering and Structural Dynamics*, 33, 903–927.
- Corradi, M., Borri, A., & Vignoli, A. (2002a). Strengthening techniques tested on masonry structures struck by the Umbria-Marche earthquake of 1997–1998. *Construction and Building Materials*, 16(4), 229–239.
- Corradi, M., Borri, A., & Vignoli, A. (2002b). Experimental study on the determination of strength of masonry walls. *Construction and Building Materials*, 17(5), 325–337.
- Da Porto, F., Guidi, G., Garbin, E., & Modena, C. (2010). In-plane behavior of clay masonry walls: Experimental testing and finite-element modeling. *Journal of Structural Engineering*, 136(11), 1379–1392.
- Del Coz Díaz, J. J., García Nieto, P. J., Martínez-Luengas, A. L., & Álvarez Rabanal, F. P. (2007). Evaluation of the damage in the vault and portico of the pre-Romanesque chapel of San Salvador de Valdediós using frictional contacts and the finite-element method. *International Journal of Computer Mathematics*, 84(3), 377–393.
- Del Piero, G. (1984). *Le costruzioni in muratura*. Berlin, Heidelberg: Springer. (in Italian).
- DM96. (1996). Decreto Ministero dei Lavori Pubblici del 16 Gennaio 1996. Norme tecniche relative ai Criteri generali per la verifica di sicurezza delle costruzioni e dei carichi e sovraccarichi. G.U. 5/2/1996, No. 29 (in Italian).
- DPCM. (2011). Direttiva del Presidente del Consiglio dei Ministri per la Valutazione e la riduzione del rischio sismico del patrimonio culturale con riferimento alle norme tecniche per le costruzioni di cui al decreto del Ministero delle infrastrutture e dei trasporti del 14 Gennaio 2008, G.U. 26/2/2011, No. 47 (in Italian).
- Drucker, D., & Prager, W. (1952). Soil mechanics and plastic analysis or limit design. *Quarterly of Applied Mathematics*, 10(2), 157–165.
- Eurocode 8 (1996) Design provisions for earthquake resistance of structures. Part 1–4: General rules—Strengthening and repair of buildings. ENV 1998-1-4: 1996. CEN, Brussels.
- Falasco, A., Lagomarsino, S., & Penna, A. (2006). On the use of pushover analysis for existing masonry buildings. In *Proceeding of the First European Conference on Earthquake Engineering and Seismology, Geneva, Switzerland, September 3–8, 2006*.
- Fioravanti, M., & Mecca, S. (Eds.). (2011). *The safeguard of cultural heritage: A challenge from the past for the Europe of tomorrow*. Florence: Firenze University Press.
- Gambarotta, L., & Lagomarsino, S. (1997). Damage models for the seismic response of brick masonry shear walls. Part I: The mortar joint model and its applications. *Earthquake Engineering and Structural Dynamics*, 26(4), 423–439.
- Hansen, E., William, K., & Carol, I. (2001). A two-surface anisotropic damage/plasticity model for plain concrete. In *Proceedings of Framcos-4 Conference 2001*.
- ICOMOS (International Council on Monuments and Sites). (2001). *Recommendations for the analysis, conservation and structural restoration of architectural heritage*. International Scientific Committee for Analysis and Restoration of Structures of Architectural Heritage, Paris, 2001.

- Ivorra, S., Pallares, F. J., & Adam, J. M. (2009). Experimental and numerical results from the seismic study of a masonry bell tower. *Advances in Structural Engineering*, 12(9), 287–293.
- Ivorra, S., Pallares, F. J., Adam, J. M., & Tomás, R. (2010). An evaluation of the incidence of soil subsidence on the dynamic behaviour of a Gothic bell tower. *Engineering Structures*, 32(8), 2318–2325.
- Kim, S., & D'Amore, E. (1999). Push-over analysis procedures in earthquake engineering. *Earthquake Spectra*, 15(3), 417–434.
- Leftheris, B. P., Stavroulaki, M. E., Sapounaki, A. C., & Stavroulakis, G. E. (2006). *Computational mechanics for heritage structures*. Southampton: WIT Press.
- Lourenço, P. B. (2005). Assessment, diagnosis and strengthening of Outeiro Church, Portugal. *Construction and Building Materials*, 19(8), 634–645.
- Lourenço, P. B., Krakowiak, K. J., Fernandes, F. M., & Ramos, L. F. (2007). Failure analysis of Monastery of Jero'nimos, Lisbon: How to learn from sophisticated numerical models. *Engineering Failure Analysis*, 14, 280–300.
- Lourenço, P. B., & Oliveira, D. V. (2007). Improving the seismic resistance of masonry buildings: Concepts for cultural heritage and recent developments in structural analysis. In *Atti del XII Convegno Nazionale ANIDIS L'Ingegneria Sismica in Italia, Pisa, 2007*.
- Lourenço, P. B., & Pina-Henriques, J. (2006). Validation of analytical and continuum numerical methods for estimating the compressive strength of masonry. *Computers & Structures*, 84, 1977–1989.
- Lucibello, G., Brandonisio, G., Mele, E., & De Luca, A. (2013). Seismic damage and performance of Palazzo Centi after L'Aquila earthquake: A paradigmatic case study of effectiveness of mechanical steel ties. *Engineering Failure Analysis*, 34, 407–430.
- NTC. (2008). Decreto Ministero delle Infrastrutture e dei Trasporti 14 Gennaio 2008. Nuove Norme Tecniche per le Costruzioni, G.U. 4/2/2008, No. 29 (In Italian).
- OPCM. (2003). Ordinanza Presidente del Consiglio dei Ministri 3274/2003. Primi elementi in materia di criteri generali per la classificazione sismica del territorio nazionale e di normative tecniche per le costruzioni in zona sismica. G.U. 8/5/2003, No. 105 (In Italian).
- Ramos, L. F., & Lourenço, P. B. (2004). Modeling and vulnerability of historical city centers in seismic areas: A case study in Lisbon. *Engineering Structures*, 26, 1295–1310.
- Romera, L. E., Hernandez, S., & Reinoso, J. M. (2008a). Numerical characterization of the structural behaviour of the Basilica of Pilar in Zaragoza (Spain). Part 1: Global and local models. *Advances in Engineering Software*, 39, 301–314.
- Romera, L. E., Hernandez, S., & Reinoso, J. M. (2008b). Numerical characterization of the structural behaviour of the Basilica of Pilar in Zaragoza (Spain). Part 2: Constructive process effects. *Advances in Engineering Software*, 39, 315–326.
- Salari, M. R., Saeb, S., Willam, K. J., Patchet, S. J., & Carrasco, R. C. (2004). A coupled elasto-plastic damage model for geo-materials. *Computer Methods in Applied Mechanics and Engineering*, 193(27–29), 2625–2643.
- Siviero, E., Barbieri, A., & Foraboschi, P. (1997). *Lettura strutturale delle costruzioni*. Milano: Città Studi Edizioni. (in Italian).
- Taliercio, A., & Binda, L. (2008). The Basilica of San Vitale in Ravenna: Investigation on the current structural faults and their mid-term evolution. *Journal of Cultural Heritage*, 8, 99–118.
- Theodossopoulos, D., & Sinha, B. (2013). A review of analytical methods in the current design processes and assessment of performance of masonry structures. *Construction and Building Materials*, 41, 990–1001.
- William, K. J., & Warnke, E. D. (1975). Constitutive model for the triaxial behaviour of concrete. In *Proceeding of the International Association for Bridge and Structural Engineering, Bergamo, Italy, 1975*.
- Zucchini, A., & Lourenço, P. (2007). Mechanics of masonry in compression: Results from a homogenisation approach. *Computers & Structures*, 85(3–4), 193–204.
- Zucchini, A., & Lourenço, P. B. (2002). A micro-mechanical model for the homogenisation of masonry. *International Journal of Solids and Structures*, 39, 3233–3255.